Journal of Hydrology: Regional Studies 40 (2022) 101003

Contents lists available at ScienceDirect

Journal of Hydrology: Regional Studies

journal homepage: www.elsevier.com/locate/ejrh

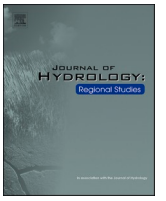

# Assessment of the WRF-Hydro uncoupled hydro-meteorological model on flashy watersheds of the *Grande Terre* tropical island of New Caledonia (South-West Pacific)

Arnaud Cerbelaud [a,*], Jérôme Lefèvre [a], Pierre Genthon [b], Christophe Menkes [a]

[a] *ENTROPIE, IRD/Université de la Réunion/Université de Nouvelle-Calédonie/CNRS, Ifremer, Nouméa, New Caledonia*
[b] *UMR 050 HydroSciences Montpellier, Université de Montpellier/CNRS/IRD, Nouméa, New Caledonia*

ARTICLE INFO

*Keywords:*
New Caledonia
Hydrological modeling
WRF-Hydro
DDS parameter adjustment
Rainfall spatial interpolation
Hydrograph separation

ABSTRACT

*Study region:* Six watersheds of the main island of New Caledonia.
*Study focus:* In the context of a projected reduction of extreme precipitation events by ~ 20% by 2100 combined to large land cover variability, a distributed hydrological approach was adopted over New Caledonia. The WRF-Hydro model was implemented using a one-way WRF meteorological forcing, with rainfall being spatially interpolated from rain gauge observations using the Thiessen polygon and IDEW methods. The Dynamically Dimensioned Search algorithm was applied for calibration on three contrasted flash-floods. Two-year validation allowed the dynamics of the watersheds to be studied and compared.
*New hydrological insights for the region:* Good results in terms of Nash-Sutcliffe efficiency were reached on all watersheds (NSE $\geq$ 0.6). WRF-Hydro showed consistent water budget components for two flash-floods with 90% correlation between simulated and observed runoff coefficients of all basins. Adjusted physical parameters matched known watershed morphological and hydrological features. Both methods of rainfall interpolation produced similar NSE but strongly different water distributions, with simulated soil moisture changes varying by up to 60% during flash-floods. Spatial patterns of soil moisture and flood decomposition led to improved understanding of watershed behavior and to a revision of infiltration properties for one of them. Overall, WRF-Hydro proved to be a suitable framework to better understand hydrological processes and efficiently handle prospective modifications of New Caledonia's land cover and climate regimes.

## 1. Introduction

As a result of large spatial heterogeneities, small tropical mountainous islands present pitfalls for hydrological modeling (Fares, 2008). Due to the reduced size of watersheds, to the slope of upstream catchments and to occurrence of extreme events such as tropical depressions, they are prone to flash floods (Strauch et al., 2015) which can be harmful for cities generally located on coastal plains. Moreover, floods transport sediments, chemical and biological components that can impact aquatic life (Richmond et al., 2007; David et al., 2010) and human health (e.g. Bierque et al., 2020). Some success in modeling these flash floods were obtained by adjustment of lumped statistical models (Wotling, 2000; Charlier et al., 2008; Desclaux et al., 2018). However, extension of these models to other

* Correspondence to: Onera, The French Aerospace Lab, France.
*E-mail address:* arnaud.cerbelaud@onera.fr (A. Cerbelaud).

https://doi.org/10.1016/j.ejrh.2022.101003
Received 12 July 2021; Received in revised form 14 January 2022; Accepted 15 January 2022
Available online 19 January 2022

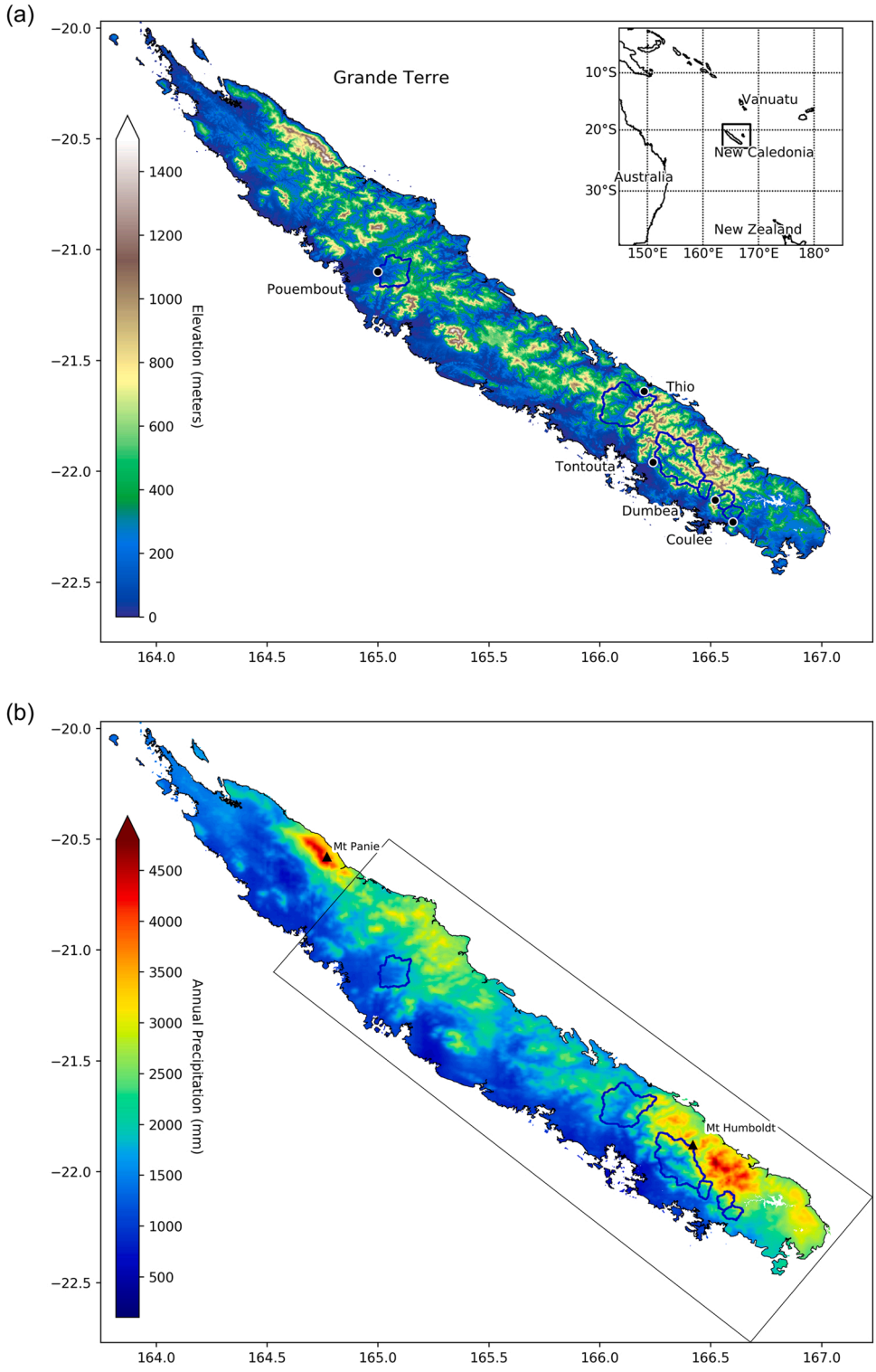


**Fig. 1.** a. (Top) Location and orography of *Grande Terre*, New Caledonia (Source: 50 m BDALTI-NC, www.georep.nc, provided by the Government of New Caledonia); b. (Bottom) Annual mean rainfall (mm) from 1990 to 2000 derived from daily rain gauge observations using the AURELHY interpolation technique (Source: *Météo-France*; Bénichou and Le Breton, 1987). The six watersheds under scope are delimited with blue lines. Soils properties and land cover within the tilted rectangular box are detailed in Fig. 2.

catchments especially to ungauged catchments is problematic (Hingray et al., 2015; Beck et al., 2016). Moreover, comparison of lumped model parameters to actual catchment properties can be confounding (Beven, 2000).

On the other hand, with the flourishing of fine spatial resolution and high frequency satellite data (Moradkhani and Sorooshian, 2009) leading to a growing availability of distributed data on rainfall, land cover, soil properties and meteorological parameters, physics-based distributed hydrological models tend to be more and more used. They allow to address the question of water resource and of distribution of water in soils (Smith et al., 2012). Moreover, fully coupled hydro-meteorological models such as the WRF/WRF-Hydro framework (Weather Research and Forecasting; Senatore et al., 2015; Arnault et al., 2018) provide insights on the coupling between vegetation, soil and atmosphere within the hydrological cycle, which is required to understand the consequences of climate change. For example, WRF-Hydro's structure relies on the Noah-MP Land Surface Model (Niu et al., 2011) for vertical routing

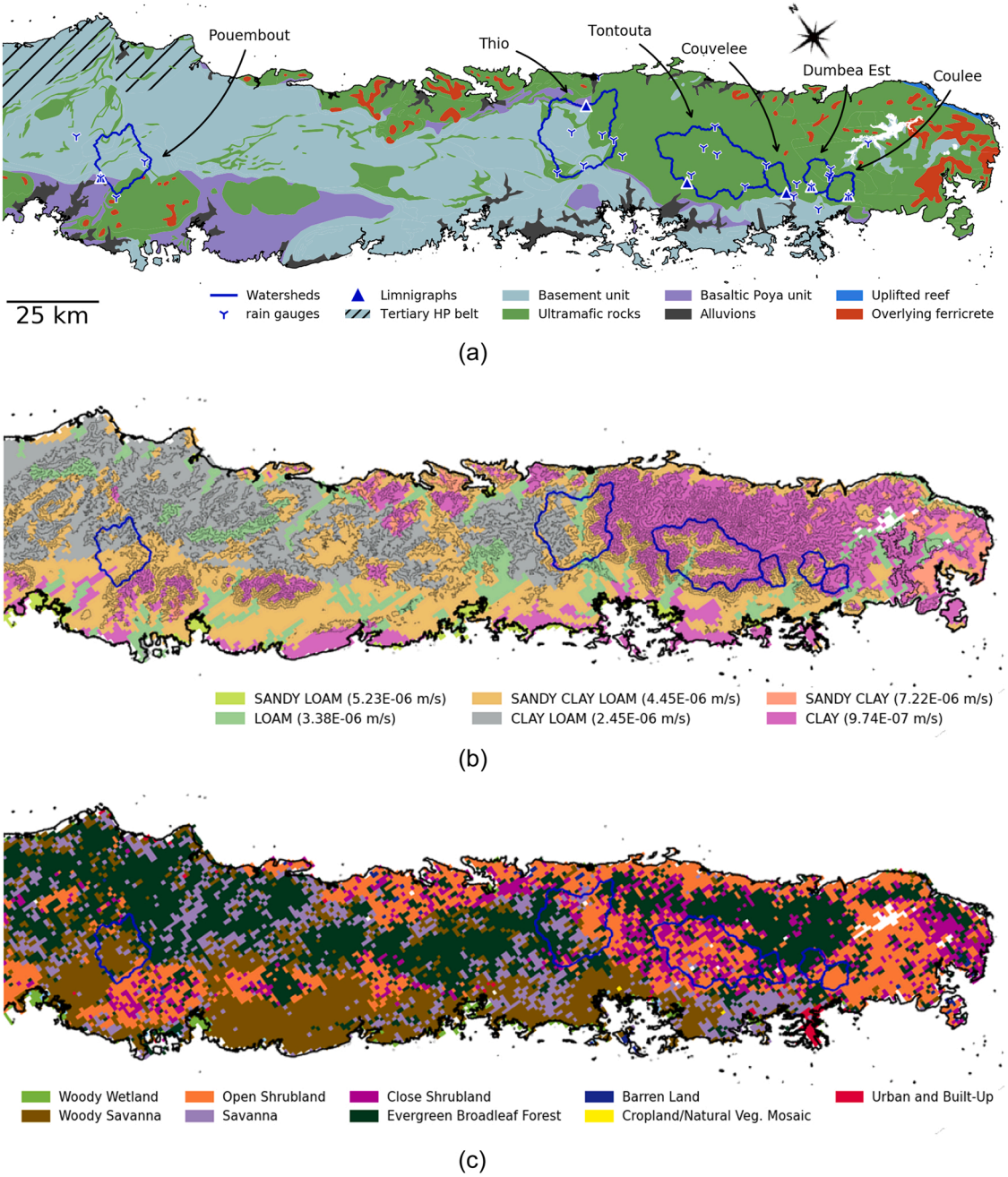


**Fig. 2.** a. (Top) Lithological; b. (Middle) Soil type with reference hydraulic conductivity; c. (Bottom) Land cover. Maps of the study area with watershed boundaries and location of rain and stream gauges.
Data sources are respectively: a. Maurizot and Vendé-Leclerc (2012); b. Fritsch (2012); c. Lafarge et al. (2014).

of water, i.e. computation of soil moisture and partition between surface runoff, infiltration and water withdrawal by vegetation. Extreme events may be simulated in a consistent way and closely analyzed thanks to coupled and distributed models.

However, at the scale of a small island, these models need to work at a resolution close to 1 km, which is presently hardly achievable due to computer power limitations. A first step to circumvent such issue can be partial decoupling of models (Rummler et al., 2019). The WRF/WRF-Hydro/Noah-MP framework allows such a decoupling. Indeed, the hydrological component WRF-Hydro can be run offline with external rainfall data.

Arnaud et al. (2002) and references therein emphasized the need of reliable high-resolution rainfall data to compute accurate peak flows and runoff volumes with a distributed model. Fares et al. (2014) ran the HL-RDHM in the Hanalei watershed in Hawaii using rainfall and soil data generated by an external software and concluded that best results were obtained with a $1 \times 1$ km$^2$ resolution for rainfall and soil moisture. Degraded results were only achieved when a coarser resolution of $2 \times 2$ km$^2$ or $4 \times 4$ km$^2$ was adopted. Camera et al. (2020) used WRF-Hydro in coupling with both observed precipitation and ERA-Interim precipitation reanalysis at a $1 \times 1$ km$^2$ resolution in Cyprus, which is a mountainous island also affected by extreme precipitation events in Mediterranean climate. They found that fair Nash–Sutcliffe efficiencies (NSE) coefficients were obtained with observed precipitations but that some basins returned negative NSE with modeled precipitation, which emphasizes the need of reliable precipitation at a fine resolution.

The *Grande Terre* island of New Caledonia is located in the SW Pacific (Fig. 1a), at the edge of the South Pacific Convergence Zone (SPCZ) in the cyclonic area of the South Pacific, and is subject to a mild tropical climate (Dutheil et al., 2020a, 2020b). It is strongly influenced by El Niño-Southern Oscillation (ENSO) on interannual timescales (Dutheil et al., 2019). It is characterized by a central mountain range and a strong asymmetry between its humid East Coast directly affected by tropical depressions and the drier western one (Fig. 1a; Terry and Wotling, 2011; Dutheil et al., 2020a, 2020b). It also presents strong contrasts in soil properties between ultramafic rocks allowing water storage in aquifers, mainly located in the South, and metamorphic volcano-sedimentary rocks generally devoid of aquifers, with strong impact on low flow regimes (Fig. 2a; Frysou, 2008). In the context of climate change, Dutheil et al. (2020b) found using fine-scale atmospheric WRF simulations that the frequency and intensity of extreme precipitation events over New Caledonia will likely be reduced by $\sim$ 20% on average by 2080–2100 under Representative Concentration Pathway (RCP) 8.5 scenario. Regional contrasts could even reach up to 40% reduction in the South of the Island. In order to anticipate the effects of such drastic projected drying on water resources while accounting for New Caledonia's large land cover variability in space and time, a suitable distributed hydrological modeling framework needs to be implemented. Desclaux et al. (2018) showed that lumped hydrological models such as GR4H were well-suited for ultramafic watersheds in the South East of New Caledonia and that adjustment of model on a 7–10 year-period was required to account for the effects of wildfires and ENSO. Effects of fire can be introduced in a distributed model by changing soil and land surface properties while large scale climate variabilities can be introduced in regional atmospheric models as boundary conditions. Despite lumped hydrological models' great scores at reproducing observed runoff, one major drawback of such compartment models is their absence of physical comprehension of mechanisms at work in the observed river outflows. The goal of this work is hence to derive physical parameters of studied watersheds and enhance hydrological knowledge of New Caledonia basins using WRF-Hydro. Because of the number of model parameters as well as the significant interactions between some of them, calibration of hydro-meteorological distributed models represents a considerable challenge. In this context, automatic methods specifically designed for hydrological purposes like the DDS algorithm (Dynamically Dimensioned Search; Tolson and Shoemaker, 2007) were shown to quickly converge towards optimal setting of model parameters for complex models (Arsenault et al., 2014), including WRF-Hydro.

Here we explore the sensitivity of the DDS calibration process and the resulting performances of WRF-Hydro with regards to the rainfall forcing as well as to the ability of the modeling system to reflect consistent hydrological behaviors. Model performances were assessed with discharge data from six contrasted watersheds located on various geological basement rocks and mainly in the southern part of the *Grande Terre* island. The outputs of the WRF-Hydro model were eventually used to illustrate and understand components of the hydrographs such as baseflow and quickflow giving indications on the functioning of the watersheds. As mentioned by Camera et al. (2020), small watersheds haven't been much studied with WRF-Hydro and the model was seldom forced with observed rainfall. Our study thus also contributes to improving this field of expertize in the WRF-Hydro community. The paper is organized as follows. In Sections 2 and 3, the studied area and the model are described including the forcing and calibration strategies; Section 4 presents the results, which are discussed in Section 5. Conclusive statements are eventually delivered in Section 6.

## 2. Study area

Approximately 400 km long and 50 km wide, *Grande Terre* is the main island of New Caledonia. Its topography is dominated by a central mountain range 800 m high on average (Fig. 1a). The two highest peaks are located on the steeper eastern side, with *Mont Panié* (1628 m) in the North and *Mont Humboldt* (1618 m) in the South.

New Caledonia hosts both temperate and tropical climate features. Its meteorological cycle is strongly impacted by the seasonal movement of the SPCZ with a warm, rainy season in austral summer and a comparatively colder and drier season in winter (Ceccarelli et al., 2013; Payri et al., 2019). With high average annual rainfall (around 1850 mm), water supply is globally abundant. Tropical cyclones also affect New Caledonia with $\sim$ 1 cyclone/year in the New Caledonia Exclusive Economic Zone. Large-scale climate fluctuations influence New Caledonia's climate with wetter than normal summer during La Niña and drier than normal (up to 20–30%) during El Niños. El Niño events strongly increase wildfire risk (Barbero et al., 2011; Lefèvre et al., 2010). Overall, water is regarded as a vulnerable resource since around 70% of the total rainfall occurs within approximately 50 days (Moron, 2016), mainly during the first quarter of the year. New Caledonia mainland's orography strongly sculpts the rainfall distribution (Fig. 1b). Indeed, higher precipitation rates are observed in the East due to the significant obstacle formed by the mountain chain to the trade-wind flow (Terry and

**Table 1**
Physical and hydrological features of studied watersheds, from Alric (2009). The Coulée, Dumbea Est, Couvelée and Tontouta watersheds are located on ultramafic basement, as well as part of the Thio watershed. The Pouembout watershed is located on metamorphic (mostly micaschist) basement.

| | Runoff coefficient (%) | Median flow rate ($m^3 s^{-1}$) | Recession time (days) | Median annual rainfall (mm) | Median altitude (m) | Median slope (%) | Hydraulic length (km) | Area ($km^2$) | Maximum Strahler Stream Order | Open shrubland area (%) | Dense vegetation area (%) |
|---|---|---|---|---|---|---|---|---|---|---|---|
| Coulée | 61 | 0.92 | 43 | 2341 | 329 | 31 | 11 | 44 | 3 | 32 | 61 |
| Dumbéa Est | 81 | 1.22 | 63 | 2717 | 492 | 32 | 12 | 60 | 3 | 24 | 74 |
| Couvelée | 41 | 0.54 | 97 | 2027 | 465 | 46 | 12 | 40 | 3 | 8 | 90 |
| Pouembout | 27 | 0.67 | 81 | 1576 | 250 | 21 | 34 | 180 | 5 | 8 | 33 |
| Thio | 57 | 3.47 | 68 | 1571 | 390 | 30 | 34 | 345 | 5 | 14 | 59 |
| Tontouta | 53 | 5.72 | 120 | 1761 | 519 | 41 | 38 | 385 | 5 | 28 | 66 |

Wotling, 2011; Dutheil et al., 2020a, 2020b).

As a result, most watersheds of *Grande Terre* are characterized by a strong East West contrast. They are steep and of limited extension, a few hundred km$^2$ at the maximum. Watersheds from the West coast end in an alluvial plain, which is not the case for the East coast. However, this effect is alleviated by the distribution of gauging stations, which are located upstream of the alluvial plain in the West coast. Rivers of Grande Terre present both flash floods resulting from extreme rainy events of the tropical climate and of the limited size of watersheds and severe low flows resulting from climate variability and from the lack of significant aquifers able to sustain river flow during dry periods. New Caledonia is surrounded by a shallow lagoon, the second largest in the world, and recognized as a UNESCO world heritage site due to its exceptional biodiversity.

One third of New Caledonia's basement consists in ultramafic rocks formed by alteration of peridotite, which are mostly concentrated in the southern part of *Grande Terre* (Fig. 2a). Soils resulting from weathering of these parent rocks include high levels of iron and magnesium, as well as several other metals such as nickel, chromium and cobalt. Such ground composition combined to mining activities causes metal-rich sediment transport downstream into rivers and eventually into the lagoon, especially during flash floods, directly impacting the reef barrier (Fig. 7 from Dupouy et al., 2018). Land cover on the upstream of the gauging stations consist of evergreen forests and shrub on peridotite basement or woody savanna on micaschists (Fig. 2c) both resulting from degradation of the initial forest due to wildfires. New Caledonia's great spatial variability in terms of land cover likely leads to complex hydro-meteorological mechanisms and feedbacks between land and the troposphere, although there is no specific study on that aspect.

In this study, six watersheds of various size and composition were examined (Fig. 2). The choices of the watersheds were dictated by the quality of long-term homogeneous data. Names, physical and hydrological features of these watersheds are shown in Table 1.

## 3. Material and methods

### 3.1. The WRF-Hydro/Noah-MP LSM modeling system

The Noah-Multiparameterization land surface model (LSM) is a spatially distributed 1-D model which solves the vertical routing of surface and subsurface water flow in response to an atmospheric forcing, based on four soil layers down to a maximum 2 m depth, with default spanning 0–0.1 m, 0.1–0.3 m, 0.3–0.6 m and 0.6–1 m. Soil water content dynamics are based on Richard's equation (Chen et al., 1996). The surface energy flux components, the gravitational drainage at the bottom soil layer and the partitioning of surface water (sum of rainfall reduced by the evaporation) into infiltration and surface runoff are also computed thanks to an ensemble of parameterization patterns (Fig. 3, see Niu et al., 2011, for details).

Since Noah-MP LSM neglects the horizontal exchanges of water, it needs to be complemented with lateral flow algorithms in order to give accurate simulation of the hydrologic cycle. WRF-Hydro is a fully distributed hydro-meteorological model that can be used for flash flood prediction, seasonal forecasting of water resources and land-atmosphere coupling studies (Gochis and Chen, 2003; Gochis et al., 2013). It was originally conceived as a coupling framework to facilitate the combined use of the WRF model and pieces of terrestrial hydrological models. It is now a stand-alone hydrological modeling architecture that can complement Noah-MP by describing lateral routing of surface and subsurface water as well as groundwater storage. It solves specifically for the saturated subsurface flow, the 2-D overland water flow, the aquifer recharge/discharge and the 1-D channel flow (Fig. 3).

In WRF-Hydro, surface flow occurs when the surface water level of a specific grid cell exceeds a maximum retention depth while subsurface flow is activated when maximum humidity capacity is exceeded in a given soil layer. Ponded water depths can be subject to future infiltration and evaporation (vertical routing from Noah-MP). The 2-D overland flow is routed across terrain elements according

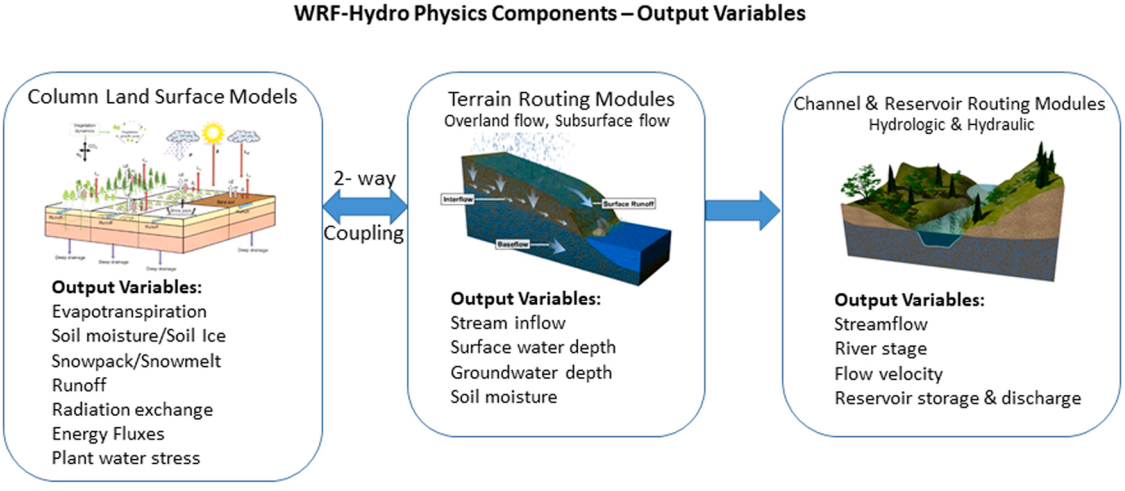


**Fig. 3.** Conceptual scheme of the WRF-Hydro/Noah-MP framework.
(Source: NCAR, https://ral.ucar.edu/sites/default/files/public/WRFHydroPhysicsComponentsandOutputVariables).

to the topography. When reaching grid cells identified as 'channel', surface water in excess of the local retention depth is passed to the channel model. In this study, the 2-D surface flow and the 1-D flow in the channels were computed with the diffusive wave equation, which is an approximation for the Saint-Venant equations that correspond to the shallow water models used in hydrology (Hingray et al., 2015). Subsurface flow is computed in soils as a function of hydraulic gradients resulting from the topography, taking into account the saturated soil depth and hydraulic conductivity (Gochis et al., 2013).

With $P$ the precipitation rate, $Q$ the surface runoff rate and $I$ the soil infiltration rate (all three in mm $s^{-1}$), the surface water budget equation at each time step $t$ is $Q(t) = P(t) - I(t)$. In the WRF stand-alone version, this infiltration excess $Q$ is removed from the model. In WRF-Hydro, it is horizontally redistributed and may infiltrate at a different time and location. The infiltration rate $I(t)$ is computed as an increasing function of the liquid soil moisture deficit of the soil column $D(t)$ (in m):

$$I(t) = P(t)\ \frac{D(t)\ \left[1 - e^{-KDT\ \delta t}\right]}{P(t)\delta t + D(t)\ \left[1 - e^{-KDT\ \delta t}\right]} \tag{1}$$

$$\text{with } KDT = REFKDT\ \frac{DKSAT}{REFDK} \text{ the infiltration coefficient } \ (\text{in } \ \text{day}^{-1}) \tag{2}$$

and

$$D(t) = \sum_{i=1}^{4} \Delta Z_i\ (SMC_{MAX} - SMC_i(t)) \tag{3}$$

$\delta t$ is the model time step (in days), $\Delta Z_i$ the soil layer's thickness (in m), $SMC_{i\ (MAX)}$ the (maximum) soil moisture content of layer $i$ ($i = 1 \ldots 4$, in $m^3\ m^{-3}$, spatially variable), DKSAT the saturated soil hydraulic conductivity (in m $s^{-1}$, spatially variable), REFDK the reference value for the saturated soil hydraulic conductivity (in m $s^{-1}$, default value $5\ .\ 10^{-6}$ m $s^{-1}$) and REFKDT the surface infiltration coefficient (in $day^{-1}$). The values of REFDK and REFKDT are constant on the whole domain.

The computation of groundwater drainage assumed to follow free gravitational drainage allows determining the aquifer content below the soil column.

$$Q_{drained}(t) = SLOPE.DKSAT.\left[\max\left(0.01, \frac{SMC_4}{SMC_{MAX}}\right)\right]^{2.BEXP+3} \tag{4}$$

It thus directly depends on the SLOPE coefficient as well as on DKSAT, BEXP (the pore size distribution index), $SMC_4$ and $SMC_{MAX}$. In this work, the simple "pass-through" option was used, which means that total basin drainage from the base of the 2 m soil column (baseflow flux) is equally redistributed among all channel pixels.

Parameters controlling the hydrograph volume are mostly the infiltration coefficient KDT and the maximum soil moisture content $SMC_{MAX}$, via the liquid soil moisture deficit of the soil column $D(t)$. Parameters controlling the hydrograph shape are mainly the 2D overland flow roughness factor (OVROUGHRTFAC) and Manning's coefficient for channel roughness (MANN). Indeed, surface roughness plays an important role in transmitting infiltration excess water to channel networks. Plausible parameter ranges are

**Table 2**
a. (Top) Typical range of WRF-Hydro's calibrated parameters (Gochis et al., 2013). KDT range results from values of REFKDT, DKSAT and REFDK; b. (Bottom) Default values for Manning's n and 2D overland roughness coefficients in WRF-Hydro for this study.

(a)

| | **REFKDT ($day^{-1}$)** | **DKSAT (m $s^{-1}$)** | **KDT ($day^{-1}$)** | **BEXP** | **SLOPE** | **OVROUGHRTFAC** | **MANN** | **$SMC_{MAX}$ ($m^3\ m^{-3}$)** |
|---|---|---|---|---|---|---|---|---|
| *Description* | (i) Surface infiltration coefficient | (ii) Saturated soil hydraulic conductivity | Infiltration coefficient from (i) and (ii) | (iii) Pore size distribution index | (iv) Percolation coefficient | (v) 2D overland flow roughness factor | (vi) Manning's factor for channel roughness | (vii) Maximum soil moisture content |
| *Reference range* | 0.1–10 | Dependent on soil texture $10^{-6}$–$10^{-5}$ | Dependent on soil texture 0.1–10 | Dependent on soil texture 0.1–5 | 0.1–1 | Multiplier to apply to the following range: 0.01–0.20 | Multiplier to apply to the following range: 0.01–0.15 | Dependent on soil texture 0–1 |

(b)

| *Strahler Stream Order* | **Manning's n for channel roughness** | *USGS categories adapted to New Caledonia* | **Overland flow roughness coefficient** |
|---|---|---|---|
| 1 | 0.14 | Open shrubland | 0.055 |
| 2 | 0.12 | Close shrubland | 0.200 |
| 3 | 0.09 | Evergreen broadleaf forest | 0.200 |
| 4 | 0.09 | *W*oody savanna and savanna | 0.055 |
| 5 | 0.07 | Dryland cropland | 0.035 |
| 6 | 0.06 | Barren land | 0.035 |
| 7 | 0.03 | Playa | 0.010 |

displayed in Table 2a of Section 3.4. We note here that, as with many physics-based modeling approaches, there can be modest interactions between some of these parameters.

### 3.2. Meteorological forcing and data sources

The WRF-Hydro model needs to be provided with atmospheric forcing. Here, we used the WRF model (Skamarock et al., 2008) widely used in the atmospheric science community. WRF was adjusted to the South Pacific and New Caledonia area in previous studies (Jourdain et al., 2011; Lefèvre et al., 2010; Dutheil et al., 2020a, 2020b; Jullien et al., 2014). It allows providing surface atmospheric state variables (air temperature, surface pressure, specific humidity, horizontal wind components at 10 m, downward incoming shortwave and longwave radiation and rainfall rate) to force WRF-Hydro and Noah-MP in offline mode. The method exposed in Lefèvre et al. (2010) and Dutheil et al. (2020a, 2020b) was used for downscaling WRF results to a spatial resolution of $4 \times 4$ km$^2$. Hourly simulation outputs were used to perform the calibration and validation of WRF-Hydro.

While atmospheric states from WRF were proven appropriate on climatological timescales and weather regime statistics compared to observation over New Caledonia (Dutheil et al., 2020a, 2020b; Lefèvre et al., 2010), the day-to-day rainfall variability was not as satisfactory and prone to large errors compared to other surface quantities, like temperature, humidity or wind. It is known that precise simulation of rainfall events with such mesoscale weather models is still challenging (Xu et al., 2019; Cuo et al., 2011; Kobold and Suselj, 2005). As accurate precipitation data in terms of volume and timing are crucial to hydrological modeling, hourly observations from the 24 tipping bucket rain gauges indicated on Fig. 2a were preferred over the model rainfall outputs. Model calibration and validation of simulated discharge were performed using data from the reference stream gauge of each watershed (Fig. 2a). Stream and rain gauge data were provided by *Direction des Affaires Vétérinaires, Alimentaires et Rurales* (DAVAR) which administrates and handles the hydrological network in New Caledonia. Additional rain gauges from *Météo-France* were also used to force the selected watersheds.

### 3.3. Model implementation and evaluation

#### 3.3.1. Rainfall spatial interpolation

Because of the sparse spatial distribution of the rainfall stations and strong influence of orography on precipitation patterns (Fig. 1), two rainfall spatial interpolation methods were tested in this study. The well-known Thiessen polygon method was used on all six watersheds. It consists in attributing a specific area of influence to each rain gauge depending on the overall gauge network over the related catchment (Fig. 4). In specific terms, each grid point of the LSM inside a given polygon (Voronoï polygons) receives the same amount of precipitation as the associated rain gauge. A second method for rainfall partitioning was evaluated based on the inverse distance and elevation weighting algorithm (IDEW; Masih et al., 2011) for sensitivity tests. It was implemented on three watersheds for it had already proven to perform well compared to other standard methods of rainfall spatial interpolation. However, previous works found that it performed only marginally better than the Thiessen polygon method with lumped models in New Caledonia (Desclaux et al., 2018). Hence the simpler Thiessen method was kept for gauge interpolation in most of this study. The mathematical form of the equation used in IDEW to calculate the interpolated rainfall $\widehat{p}_{(i,j),t}$ at grid point *(i,j)* and time $t$ from hourly time series data of k$^{\text{th}}$ rain gauge $p_{k,t}$ over all $n$ gauges is:

$$\widehat{p}_{(i,j),t} = \sum_{k=1}^{n} p_{k,t} \left[ \frac{1}{D_{(i,j)}} \frac{W}{\left(d_{k,(i,j)}\right)^{\alpha}} + \frac{1}{Z_{(i,j)}} \frac{1-W}{\left(\Delta z_{k,(i,j)}\right)^{\beta}} \right] \tag{5}$$

with $d_{k,(i,j)}$ the distance (in m) between k$^{\text{th}}$ rain gauge and grid point *(i,j)*, $\Delta z_{k,(i,j)}$ the difference in altitude (in m) between the two, and $D_{(i,j)} = \sum_{k=1}^{n} \frac{1}{\left(d_{k,(i,j)}\right)^{\alpha}}$ and $Z_{(i,j)} = \sum_{k=1}^{n} \frac{1}{\left(\Delta z_{k,(i,j)}\right)^{\beta}}$ the normalization terms.

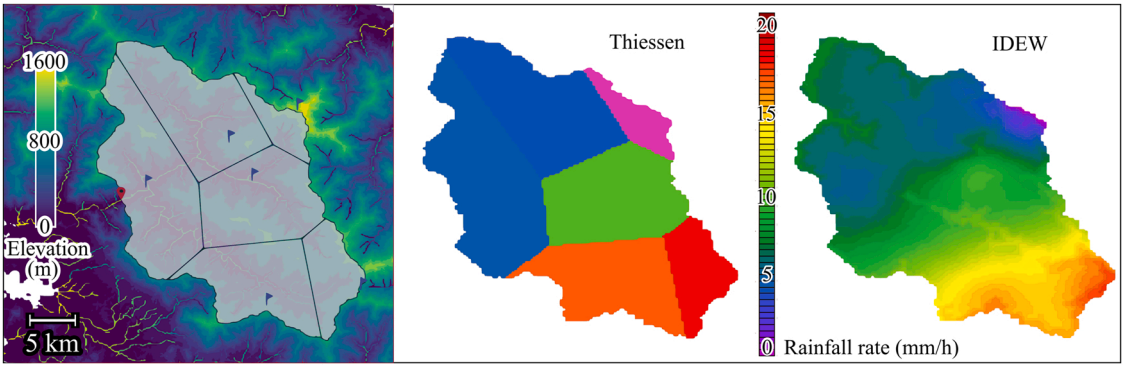


**Fig. 4.** Left panel: Location of rain (blue flags) and stream (red dots) gauges and resulting Thiessen Polygons over topography on the Tontouta watershed. Right panel: Example of rainfall spatial interpolation at a given time step (one hour); left image in the panel corresponds to the Thiessen polygon method and right one displays the IDEW algorithm. Rainfall is in mm h$^{-1}$.

The coefficients recommended by Masih et al. (2011) were used here, i.e. $W = 0.8$, $\alpha = 2$ and $\beta = 1$. These values are fairly close to the optimal set Desclaux et al. (2018) determined using the lumped model GR4H over four New Caledonia watersheds ($W = 0.8$, $\alpha = 1.5$ and $\beta = 0.5$).

### 3.3.2. Validation metrics

The normalized version of the root mean squared error, i.e. the Nash-Sutcliffe efficiency (NSE) coefficient most commonly used for evaluation of hydrological models, was used as a performance indicator along with its log transformed version. The Kling-Gupta efficiency (KGE; Gupta et al., 2009) criterion was also used in particular for calibration purposes. These efficiency criteria have different assets and drawbacks depending on their use, such as calibration or performance analysis of simulations $x_{s,t}$ faced with observations $x_{o,t}$, $t = 1…N$. They are computed as follows:

$$NSE = 1 - \frac{\sum_{t=1}^{N} (x_{o,t} - x_{s,t})^2}{\sum_{t=1}^{N} (x_{o,t} - \overline{x}_o)^2} \quad \text{i.e.} \quad NSE = 1 - \frac{RMSE^2}{{\sigma_o}^2} \tag{6}$$

$$KGE = 1 - \sqrt{(r-1)^2 + (\alpha - 1)^2 + (\beta - 1)^2} \tag{7}$$

with $r$ the linear correlation coefficient between $x_s$ and $x_o$, $\alpha = \frac{\sigma_s}{\sigma_o}$, $\beta = \frac{\overline{x}_s}{\overline{x}_o}$. Quantities $\overline{x}_o$, $\overline{x}_s$, $\sigma_o$ and $\sigma_s$ are the mean and standard deviation of the observed and simulated streamflow values respectively.

While the NSE exhibits a strong sensitivity towards peak flows and provides little information on systematic model biases, the log-transformed NSE provides more information on the quality of low water simulations. KGE was used in this study as an alternative criterion that can help reduce model calibration problems. However, it is important to have in mind that it was never intended by their authors as an improved measure of model performance (see Gupta et al., 2009).

## 3.4. WRF-Hydro setup and calibration procedure

The approach adopted here involves forward coupling of the WRF-Hydro model by forcing it with a 2 year-long atmospheric simulation computed with WRF (except for rainfall). WRF-Hydro was run using a 50 m Digital Elevation Model (DEM) generated from the BDALTI-NC database provided by the New Caledonia Government, land cover generated from MODIS (500 m) with classification of vegetation types based on local forestry expertize (Lafarge et al., 2014) and soil type data at 2000 m resolution, adapted from the Atlas of New Caledonia (Fritsch, 2012) to fit USGS categories (Lafarge et al., 2014). The hydrological routing grid was chosen at 100 m resolution, while a cell spacing of 200 m for the Noah-MP LSM was implemented. Both were prepared under GRASS GIS 7.6.0. The time-step was set to 900 s for the land surface model (vertical routing). To maintain model stability and prevent numerical dispersion of overland flood waves, a conservative time step of 10 s for channel and overland flow routing was chosen in this study. This value met the Courant condition criteria (CFL) for adaptive time integration schemes of the flow equations on a 100 m resolution grid. However, it needed to be decreased locally to 3 s for Thio watershed for some flood events as instabilities were still recorded when observations exceeded 4500 $m^3\ s^{-1}$.

Noah-MP LSM and WRF-Hydro require a great deal of input parameters; most of them directly dependent on either land use (e.g. type and density of vegetation) or soil type (e.g. silt, clay, loam, sand). The calibration process allows determining the optimal tunable coefficients to apply to these spatial parameters proportionally to their default values. Based on suggestions by Yucel et al. (2015), Verri et al. (2017), Rummler et al. (2019) and Camera et al. (2020), seven parameters were calibrated: (i) the surface infiltration coefficient, or soil permeability, (ii) the saturated soil hydraulic conductivity, (iii) the pore size distribution index, (iv) the percolation coefficient, (v) the 2D overland flow roughness factor, (vi) Manning's factor for channel roughness, and (vii) the maximum value for soil moisture storage. Typical range of these parameters is displayed in Table 2a. Other WRF-Hydro tables specifying parameters regarding the channel geometry, bucket model coefficients (irrelevant here with the pass-through option) and lateral surface and subsurface water routing factors were left to their default values (Gochis et al., 2013). The pore size distribution index (BEXP), the maximum soil moisture content ($SMC_{MAX}$) and the infiltration coefficient (KDT) correspond to an adjustment of soil-dependent values (through DKSAT for KDT) already introduced in the Noah-MP land surface model. The percolation (SLOPE) and soil permeability (REFKDT) parameters are spatially constant on each watershed. Both the overland flow roughness factor (OVROUGHRTFAC) and the Manning's factor for channel roughness (MANN) are multiplicative factors that apply to reference values, depending on land occupation for the former and on the Stralher order of each river reach for the latter (Gochis et al., 2013). These reference values are provided in Table 2b.

The calibration procedure based on the DDS global optimization algorithm for watershed modeling, designed by Tolson and Shoemaker (2007) was used by running the NCAR's (National Center for Atmospheric Research) workflow written by Karsten (2018). The DDS algorithm has been shown to be suitable for a great number of parameters to optimize and to rapidly converge to best calibration solutions while easily avoiding poor local optima. The scalar neighborhood size perturbation parameter (r) that defines, at each iteration, the amplitude of the random perturbation as a fraction of the range of the parameter to be modified was set at its default value of 0.2. KGE was chosen as calibration criterion and the number of iterations was limited to 100.

Each watershed was independently calibrated on three characteristic week-long storms (similarly to what was performed in Yucel

et al., 2015). The June 2012–March 2014 period was chosen for data cross-availability purposes. That range included both moderate El Niño and La Niña periods which allow to sample both dry and wet conditions in New Caledonia. In addition, it covered the seasonal cycle as well as several extreme meteorological events such as tropical depressions (e.g. Edna in February 2014). Each calibration procedure was initialized with restart files (which is critical for soil moisture initial conditions) from 9 months spin-up runs made with default values for all parameters. Calibration was carried out on the three events labeled as black boxes on Fig. 5 using the Thiessen polygon rainfall spatial interpolation method and the IDEW algorithm for three of the six watersheds. Event 1 was a very strong stormy event in an unusual dry period, between 2013/06/30 and 2013/07/05; event 2 was a weaker and more usual rainy event between 2013/11/30 and 2013/12/05 that induced a more moderate hydrological response; and event 3 corresponded to the Edna tropical depression in the heart of the rainy season between 2014/02/02 and 2014/02/07. All in all, the two-year simulation period and the calibration events chosen in this study allowed accounting for a fair amount of variability in the New Caledonia case.

For each watershed and method of rainfall interpolation, the three distinct parameter sets obtained by calibration on each of the three events were then used to validate the model over the June 2012–March 2014 remaining period. The best calibration set was chosen based on a multiobjective criterion consisting in the arithmetic mean of *NSE*, $NSE_{log10}$ and *KGE*, computed on the validation period. The use of such criterion was justified by the variety of patterns over which each criterion exhibits specific sensitivity to, in order to keep quality-balanced simulations. Finally, Thio watershed could not be calibrated upon event 1 because of missing streamflow data in July 2013, probably due to system malfunction caused by the storm. Initial unsatisfactory calibration of Thio over the second and third event led to a successful 24-day calibration on event 3 starting from 2014/01/15 instead of 2014/02/02.

## 4. Results

### 4.1. Performance of WRF-Hydro and calibrated parameter values

With Thiessen rainfall forcing, model performances (Table 3) concerning NSE could be considered as good, except perhaps for the Pouembout watershed, where they were only satisfactory according to Moriasi et al. (2007) criteria. The multiobjective criterion, being more sensitive to low flows, allowed better discrimination of watersheds with unsatisfactory low flow simulations as was the case for Couvelée and Pouembout.

WRF-Hydro is very sensitive to the adjustment of six parameters (Table 3; with KDT resulting from calibration of REFKDT and DKSAT). Final calibrated values of these parameters corresponded to those commonly found in the literature (Yucel et al., 2015; Verri et al., 2017; Camera et al., 2020), including high Manning values as it can be the case for woody rivers in small steep mountainous catchments (Yochum et al., 2012). The maximum soil moisture content ($SMC_{MAX}$) was found relatively stable, with the one exception of the Pouembout watershed (and to a lesser extent Couvelée), with a very large water storage capacity, affording larger soil moisture deficit (D(t), see Eqs. (1) and (3)). The pore size distribution index, the percolation and the infiltration coefficients exhibited strong variations, suggesting that some additional efforts in adjusting the spatial variability of hydraulic properties of soils, roughness and vegetation should be made. For example, Dumbéa Est and Coulée have similar environmental properties (Table 1) and share some common delineation (Fig. 2), but a striking difference in the KDT factor was observed. While usual values for KDT are in the range of 0.1–5 $day^{-1}$, this optimal timescale factor for the partition between infiltration and runoff was found in the upper bound for Coulée, but in the lower bound for Dumbéa Est. This peculiar point will be addressed in 5.1. Both Manning and overland roughness factors, two important friction parameters acting on the flood temporal dynamics during storm events, showed important differences among the six watersheds.

Significant Pearson correlations were found (Fig. 6) between some of WRF-Hydro's model parameters, the two validation criteria and the morphometric as well as the hydrological properties of the watersheds (Table 1) taken from Alric (2009). Despite the use of the

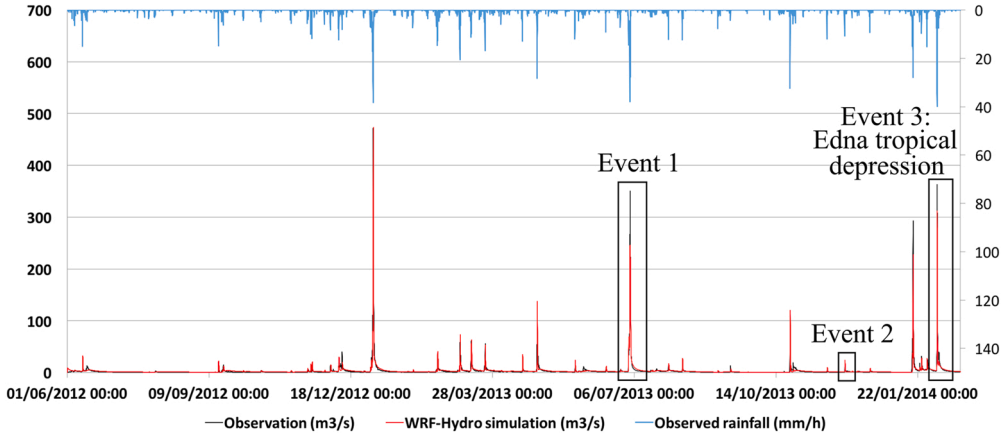


**Fig. 5.** WRF-Hydro simulated (red) and observed (black) hydrograph of Dumbéa Est watershed. Rainfall is plotted in blue along the top axis. Calibrations were carried out on the three events labeled as black boxes. Left axis for streamflow is in $m^3\ s^{-1}$ and right axis for rainfall is in mm $h^{-1}$.

**Table 3**
WRF-Hydro optimal parameters and performances obtained for each watershed from the best June 2012–March 2014 validation run following each of the three week-long calibrations (Thiessen method).

| | Performance criteria | | Infiltration/ runoff partitioning | Drainage strength | | Surface runoff strength (Friction parameters) | | Soil water holding capacity |
|---|---|---|---|---|---|---|---|---|
| | NSE | Multi Objective criterion | Infiltration coefficient KDT ($day^{-1}$) | Pore size distribution index BEXP | Percolation parameter SLOPE | Overland roughness factor OVROUGHRTFAC | Manning roughness factor MANN | Maximum soil moisture content $SMC_{MAX}$ ($m^3\ m^{-3}$) |
| Coulée | 0.61 | 0.64 | 5.0 | 3.4 | 0.98 | 0.21 | 1.65 | 0.39 |
| Dumbéa Est | 0.89 | 0.80 | 0.8 | 2.8 | 0.81 | 0.38 | 2.50 | 0.39 |
| Couvelée | 0.74 | -0.01 | 3.8 | 0.5 | 0.25 | 0.12 | 1.80 | 0.54 |
| Pouembout | 0.58 | -0.34 | 0.3 | 1.5 | 0.69 | 0.47 | 0.87 | 0.61 |
| Thio | 0.76 | 0.41 | 0.6 | 2.3 | 0.50 | 0.18 | 0.55 | 0.44 |
| Tontouta | 0.80 | 0.40 | 2.8 | 1.5 | 0.31 | 0.15 | 0.55 | 0.36 |

statistical significance levels (Fisher and Yates, 1953, denoted by stars and colors in Fig. 6), these results should be taken with caution as the size of the studied sample (six watersheds) is small. Hence only correlations greater than 0.73 (p-value = 0.1), 0.81 (p-value = 0.05) and 0.92 (p-value = 0.01) are highlighted and discussed in Fig. 6. The pore size distribution index was found fairly correlated with the SLOPE parameter, the open shrubland land occupation and the recession time (negative correlation). The maximum soil moisture content was positively correlated with the woody savanna land occupation and negatively correlated with the runoff coefficient. The SLOPE coefficient was only correlated to the recession time (negatively) and the pore size, the 2D overland roughness coefficient to woody savanna (fair correlation) while the Manning river coefficient was strongly correlated with rainfall and the hydraulic length of the basin (negative sign). The infiltration coefficient was fairly correlated to soil types. Section 5.3 discusses these results.

The two validation criteria were not correlated with the same variables: the Nash criterion, which is mainly sensitive to flood peaks, was not strongly correlated to any other variable, except maybe to the runoff coefficient. By contrast the multiobjective criterion was correlated with several independent parameters. It was strongly correlated (0.97 correlation coefficient) with the runoff coefficient of the basin and with the maximum soil moisture content (− 0.92). It was also fairly correlated with the sandy clay loam soil occurrence, the woody savanna land occupation and the pore size distribution index. Due to the correlations with the runoff coefficient and with soil parameters such as clay type that favors runoff, one can conclude that the WRF-Hydro model works better when only surface water is involved in flood generation.

### 4.2. *WRF-Hydro water budget components and consistency in hydrological behaviors*

The detailed study of major storms 1 and 3 (Fig. 5) throughout the different water components of WRF-hydro's simulations showed many interesting features. Event 1 took place during the cold season when little rainfall is usually observed and did not occur after any other significant flood. Event 3 occurred in the heart of the hot, rainy season and marked the end of a one month-long continuous rainy period. The water budget components computed by WRF-Hydro during events 1 and 3 are given in Fig. 7. As the model is conservative for the total amount of water, accumulated rainfall during these events (summing up to between 10% and 20% of the yearly amount) could thus be decomposed into surface runoff, change in soil moisture storage and groundwater outflow. As expected during an extreme rainfall window of only a few days, transpiration and evaporation were negligible. However, simulations did account for the

| | | WRF-Hydro calibrated parameters | | | | | | WRF-Hydro performance indicators | | WRF-Hydro soil type | | | WRF-Hydro land cover | | | Watersheds characteristics from Alric (2009) | | | |
|---|---|---|---|---|---|---|---|---|---|---|---|---|---|---|---|---|---|---|---|
| | | *Pore size* | *Max soil cont* | *Slope* | *2D roughness factor* | *River manning factor* | *Infil coeff* | *NSE* | *Multi* | *sandy clay loam* | *clay loam* | *clay* | *woody savanna* | *open shrubland* | *close shrubland* | *Runoff coeff* | *Recession time* | *Median rainfall* | *Hydraulic length* |
| **WRF-Hydro calibrated parameters** | *Pore size* | 1,00 | | | | | | | | | | | | | | | | | |
| | Max soil cont | -0,57 | 1,00 | | | | | | | | | | | | | | | | |
| | Slope | 0,84** | -0,08 | 1,00 | | | | | | | | | | | | | | | |
| | 2D roughness factor | 0,20 | 0,48 | 0,47 | 1,00 | | | | | | | | | | | | | | |
| | River manning factor | 0,32 | -0,08 | 0,51 | 0,26 | 1,00 | | | | | | | | | | | | | |
| | Infil coeff | 0,06 | -0,28 | 0,05 | -0,69 | 0,08 | 1,00 | | | | | | | | | | | | |
| **WRF-Hydro performance indicators** | NSE | -0,01 | -0,59 | -0,35 | -0,16 | 0,30 | -0,23 | 1,00 | | | | | | | | | | | |
| | Multi | 0,74* | -0,92*** | 0,38 | -0,21 | 0,41 | 0,22 | 0,57 | 1,00 | | | | | | | | | | |
| **WRF-Hydro soil type** | sandy clay loam | -0,67 | 0,76* | -0,41 | 0,49 | -0,15 | -0,73 | -0,04 | -0,76* | 1,00 | | | | | | | | | |
| | clay loam | -0,07 | 0,45 | 0,00 | 0,42 | -0,51 | -0,70 | -0,39 | -0,53 | 0,60 | 1,00 | | | | | | | | |
| | clay | 0,38 | -0,63 | 0,24 | -0,47 | 0,42 | 0,79* | 0,24 | 0,70 | -0,86** | -0,92*** | 1,00 | | | | | | | |
| **WRF-Hydro land cover** | woody savanna | -0,22 | 0,84** | 0,14 | 0,74* | -0,26 | -0,56 | -0,62 | -0,76* | 0,71 | 0,74* | -0,78* | 1,00 | | | | | | |
| | open shrubland | 0,82** | -0,62 | 0,67 | -0,18 | 0,26 | 0,60 | -0,11 | 0,73 | -0,94*** | -0,49 | 0,78* | -0,48 | 1,00 | | | | | |
| | close shrubland | -0,33 | -0,45 | -0,68 | -0,43 | -0,29 | 0,16 | 0,62 | 0,25 | -0,15 | -0,48 | 0,35 | -0,51 | -0,06 | 1,00 | | | | |
| **Watersheds characteristics from Alric (2009)** | Runoff coeff | 0,69 | -0,85** | 0,36 | -0,08 | 0,54 | 0,04 | 0,69 | 0,97*** | -0,59 | -0,47 | 0,58 | -0,70 | 0,57 | 0,20 | 1,00 | | | |
| | Recession time | -0,81** | 0,20 | -0,89** | -0,21 | -0,46 | -0,04 | 0,26 | -0,42 | 0,41 | -0,12 | -0,14 | 0,03 | -0,57 | 0,77* | -0,42 | 1,00 | | |
| | Median rainfall | 0,51 | -0,43 | 0,53 | 0,04 | 0,92*** | 0,30 | 0,40 | 0,70 | -0,50 | -0,72 | 0,71 | -0,55 | 0,56 | -0,07 | 0,76* | -0,47 | 1,00 | |
| | Hydraulic length | -0,28 | 0,18 | -0,45 | 0,19 | -0,86** | -0,50 | -0,11 | -0,41 | 0,42 | 0,62 | -0,61 | 0,48 | -0,42 | 0,32 | -0,45 | 0,53 | -0,86** | 1,00 |

**Fig. 6.** Pearson correlation matrix with * for coefficients > 0.73 (p-value < 0.10), ** > 0.81 (p-value < 0.05) and *** > 0.92 (p-value < 0.01).

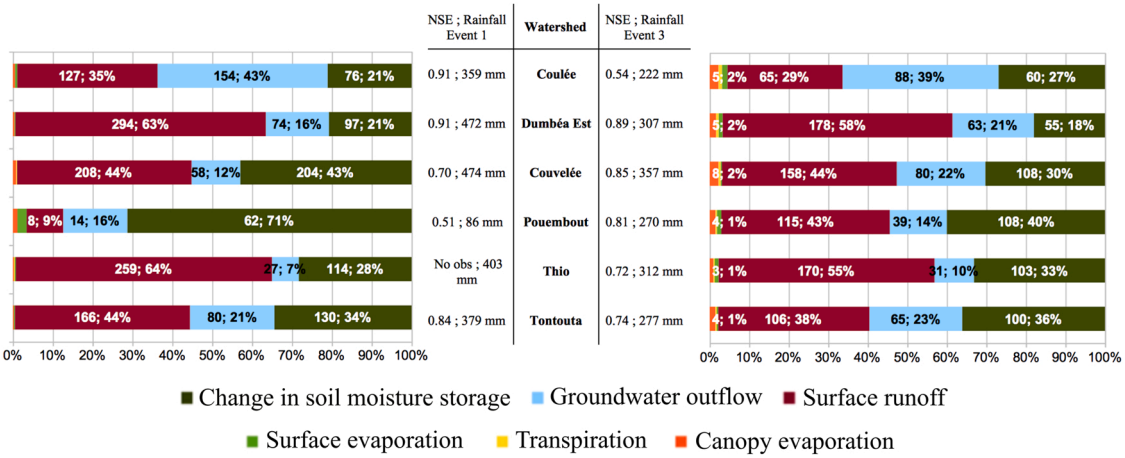


**Fig. 7.** Optimal simulated water budgets by WRF-Hydro on two flash-flood events between $t_0$ and $t_0 + 5$ days. Except for the NSE, all values are given in mm; % of total rainfall. Left panels represent the budgets for event 1 and right panels for event 3.

fact that evapotranspiration was higher during event 3, which occurred in the austral summer period. Using WRF-Hydro outputs, runoff coefficients could be computed from the sum of surface runoff and groundwater outflow.

As seen in Fig. 8, the resulting simulated runoff coefficients were in agreement with the mean runoff coefficients (Alric, 2009) of their watersheds for the two events. Indeed, there was high positive correlation between reference values of runoff coefficients (x-axis) and event computed runoff coefficients (y-axis): 0.90 for event 1 and 0.86 for event 3 (p-value $< 0.05$). The Pouembout river presented a low simulated runoff for event 1 ($\sim$ 25%), close to its mean referenced value (27%). Interestingly, it received a relatively small amount of rainfall (86 mm) that soils were mostly able to absorb, while the other watersheds received more than 350 mm. Conversely Pouembout's runoff coefficient during event 3 was 57%, which is much larger than the mean 27% referenced for this watershed. That probably corresponded to a rainfall intensity exceeding the infiltration soil capacity. Compared to other basins and especially to its neighbor Dumbéa Est, Coulée presented a very large groundwater outflow as part of its high runoff coefficient (additional discussion is provided in Section 5.1 while focusing on baseflow behavior). Couvelée was found to be able to store large amounts of water in its soil layers during both extreme rainfall events (especially during event 1 with 204 mm) along with little groundwater outflow, leading to slow return of rainwater to the stream channel. Such behavior was in agreement with its low referenced runoff coefficient (41%, Table 1) and rather high recession period (97 days, Table 1). This was supported by a high calibrated $SMC_{MAX}$ value (0.54 $m^3/m^3$), providing conditions for large moisture deficits (Eq. (3)), a large infiltration capacity during storms (KDT value of 3.8 $day^{-1}$, see Table 3

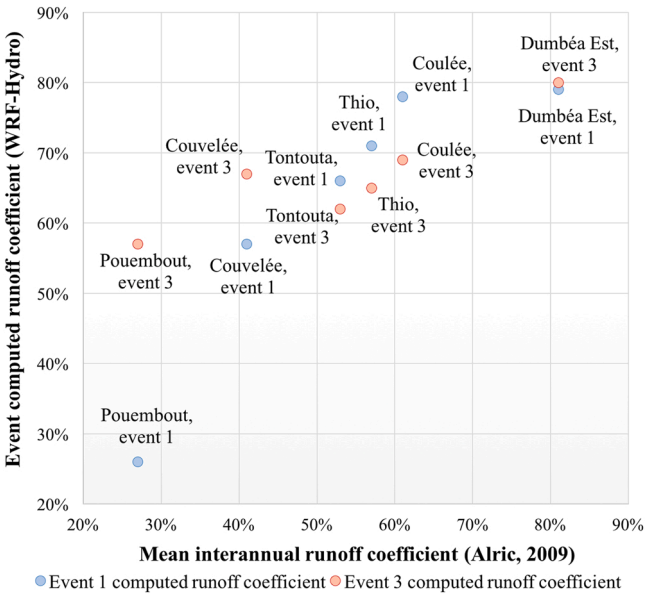


**Fig. 8.** Event computed runoff coefficients from WRF-Hydro as a function of mean interannual runoff coefficients (Alric, 2009) during two flash-flood events.

and Eq. (1)) and a low drainage strength (through low values for SLOPE and BEXP, Table 3) promoting a slowdown of the groundwater outflow in interstorm periods.

Tontouta and Thio are the two largest drainage basins with area above 340 $km^2$. They share similar runoff coefficients (~ 55%) but Tontouta has a recession time twice that of Thio (120 days, the longest of our sample, see Table 1). Fig. 7 reveals that the simulated surface runoff on Thio basin was high (> 55%) in storm periods compared to Tontouta (< 45%), but the underground runoff was higher (> 20%) for the latter compared to the former (< 10%). Just like Couvelée, this hydrological response from Tontouta could be associated with large KDT value (2.8 $day^{-1}$), small pore size distribution index (1.5) and low SLOPE parameter (0.31, Table 3) that participated in the slowdown of the subsurface and groundwater drainage and long recession time. Other differences in soil properties and spatial distribution of land cover could not be ruled out and are discussed in 5.1.

### 4.3. Hydrological response to the spatial distribution of rainfall

The changes in model performance and values of calibrated parameters between the IDEW and the Thiessen polygon rainfall interpolation methods are displayed in Table 4. Here, the sensitivity to spatial distribution of rainfall was addressed using Dumbéa Est (60 $km^2$) and Coulée (40 $km^2$), two watersheds sharing some common delineation and lithology (ultramafic), but displaying large variation in calibrated parameters (Table 3), and Pouembout (180 $km^2$), the unique river basin in this study with a metamorphic lithology. The resulting changes in water budget components for events 1 and 3 are displayed in Fig. 9.

Contrary to Thiessen, IDEW considers the difference in altitude and distance to rain gauges to interpolate precipitation data. This led to modifications in the spatial distribution of total rainfall at the basin scale in time, with more rainfall on high areas (see Fig. 4) where soils and vegetation are usually denser, and in the presence of drier downhill areas that were thus less saturated at the beginning of major events. In turn, it resulted in modifications in the water budgets, with simulated changes in soil moisture storage varying by up to 60% during flash-floods compared to Thiessen (from 97 mm to 97 + 63 mm for event 1 on Dumbéa), even if total rainfall was rather unchanged (± 5% at maximum, Fig. 9). Performances were rather similar for all watersheds using both methods. However, a higher NSE but lower multiobjective criterion was achieved on Pouembout with IDEW.

The change in spatial distribution of rainfall due to IDEW drove a robust change in calibration, in particular through KDT (Table 4), the timescale parameter controlling the partition of rainfall into surface runoff and infiltration (Eq. (1)). Using IDEW rainfall interpolation, KDT was systematically doubled indicating that more water was injected into the lower zone, reducing the overall surface flow. Since values of BEXP and SLOPE, two parameters controlling the strength of the drainage from the soil column, were reduced by half in IDEW compared to Thiessen, a possible compensation effect could be at stake: the larger the infiltration to the lower zones due to larger values of KDT, the lower BEXP and SLOPE. Furthermore, one may observe a similar compensation effect through lower surface and channel friction parameters with IDEW. Indeed, the model responded accordingly to balance lower surface flow to the drainage network so as to respect the shape of flood hydrographs. It is worth noting that $SMC_{MAX}$, the parameter describing how much water soils can store, was the only parameter to show very little sensitivity to changes in rainfall interpolation.

Since the two spatial distributions for rainfall resulted in two distinct sets of WRF-Hydro optimal parameters, sensitivity of the water budgets to these interpolation changes was also closely analyzed. From Fig. 9, increase of water storage in soils using IDEW was well captured in the watershed pair Dumbéa Est and Coulée, both responding by a large reduction in surface runoff. However, the Pouembout basin presented an opposite behavior with slightly increased surface runoff with IDEW. Such contrasted reactions in the water budgets may stem from large differences in physiography, lithology and/or land cover between basins (Table 1). As upland areas correspond in Dumbéa Est and Coulée terrestrial data to forest or close shrubland that both favor infiltration and to a clay soil that favors runoff, these results suggested that the former effect could prevail for these watersheds. In the Pouembout watershed, the presence of woody savanna uphill that is suspected to play an important role in the production and transfer of rainwater flow to downslope areas (Tramier et al., 2021) could explain part of the opposite effect.

Differences in spatial distribution of rainfall slightly altered the calibration quality as well (Table 4). For example, small basins like

**Table 4**
WRF-Hydro optimal parameters and performances obtained for each watershed from the best June 2012–March 2014 validation run following each of the three week-long calibrations (IDEW-Thiessen).

| | | Performance criteria | | Infiltration/ runoff partitioning | Drainage strength | | Surface runoff strength (Friction parameters) | | Soil water holding capacity |
|---|---|---|---|---|---|---|---|---|---|
| | | NSE | Multi Objective criterion | Infiltration coefficient KDT ($day^{-1}$) | Pore size distribution index BEXP | Percolation parameter SLOPE | Overland roughness factor OVROUGHRTFAC | Manning roughness factor MANN | Maximum soil moisture content $SMC_{MAX}$ ($m^3$ $m^{-3}$) |
| Coulée | IDEW | 0.58 | 0.56 | 8.9 | 1.9 | 0.37 | 0.07 | 1.06 | 0.38 |
| | Thies. | 0.61 | 0.64 | 5.0 | 3.4 | 0.98 | 0.21 | 1.65 | 0.39 |
| Dumbéa Est | IDEW | 0.82 | 0.76 | 2.0 | 1.5 | 0.50 | 0.63 | 0.59 | 0.38 |
| | Thies. | 0.89 | 0.80 | 0.8 | 2.8 | 0.81 | 0.38 | 2.50 | 0.39 |
| Pouembout | IDEW | 0.74 | -0.54 | 0.7 | 1.4 | 0.36 | 0.01 | 0.55 | 0.57 |
| | Thies. | 0.58 | -0.34 | 0.3 | 1.5 | 0.69 | 0.47 | 0.87 | 0.61 |

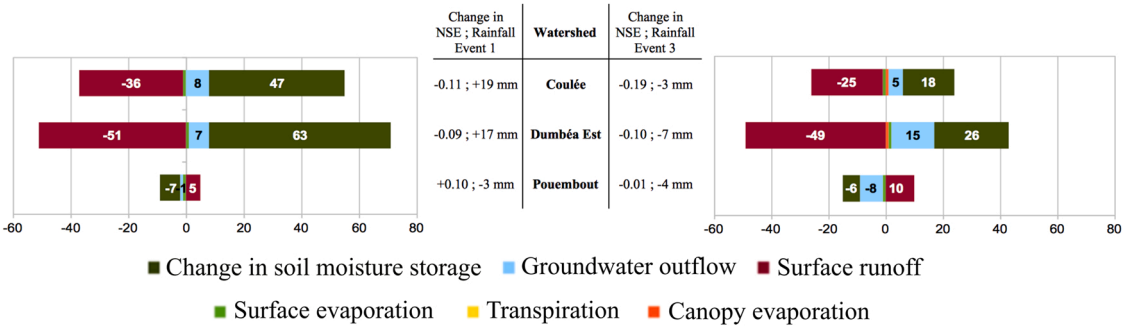


**Fig. 9.** Changes (IDEW-Thiessen) in optimal simulated water budgets by WRF-Hydro depending on rainfall spatial interpolation method on two flash-flood events between $t_0$ and $t_0 + 5$ days. Except for the NSE, all values are given in mm. Left panels represent the budgets for event 1 and right panels for event 3.

Coulée and Dumbéa exhibited somewhat lower Nash criterion when using IDEW compared with Thiessen (a small decrease, $\leq 0.07$ points on the Nash scale), while IDEW promoted a better flood prediction in the Pouembout case (Nash value of 0.74 against 0.58 with Thiessen). Pouembout observed and simulated flood hydrographs during the Edna tropical depression are shown in Fig. 10. Clearly, the hydrological response with IDEW for that basin seemed to enhance the simulated timing and shape of the flood compared with observations during that event. The slightly increased surface runoff partly induced by the IDEW parameter set, especially the very low friction parameter (0.01 for OVROUGHRTFAC, Table 4), is likely to have acted for quicker and clearly more fitting timely response for the second peak flow. By contrast, the same close inspection of the flood hydrographs for Dumbéa Est (Fig. 11) and Coulée (not shown here) indicated that a slower response with less surface runoff (light green bars) in the case of IDEW did not seem adequate for these

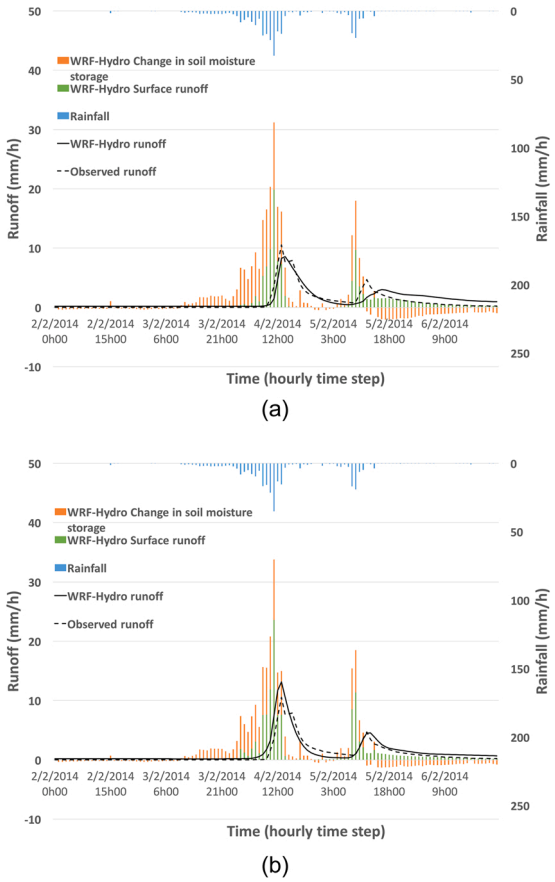


**Fig. 10.** Hourly water budget from rainfall (vertical bars), observed (dashed) and simulated (solid line) hydrograph of the Pouembout watershed depending on the rainfall interpolation method used for calibration and simulation for event 3. Panel (a) uses Thiessen interpolation and (b) uses IDEW method.

watersheds, especially in terms of flood recession behavior. That is further discussed in Section 5.2.

## 5. Discussion

### 5.1. Lessons from WRF-Hydro's hydrograph separation

Using a physics-based model allows computing the different components of a flood. Here a separation between quickflow and baseflow is proposed through one application focused on differences between Dumbéa Est and Coulée. As pointed out, both river basins share some common delineation (Fig. 2) and are thus close in terms of environmental properties and highly related. However, WRF-Hydro's calibration led to large differences in their simulated hydraulic properties and behaviors, with opposite values for the KDT timescale factor for infiltration/runoff (Table 3 and Table 4) and contrasted details in the water partition (see water budgets from Fig. 7).

Fig. 12 details and compares their respective flood hydrograph during event 1. Both watersheds reacted comparably in terms of streamflow to the extreme rainfall event (with Dumbéa Est receiving somewhat higher cumulated precipitations). As represented by the solid light blue line, WRF-Hydro however suggested different baseflow behaviors for the two watersheds. Within our framework, baseflow corresponds to the decrease of soil water content in post storm days (the baseflow curve and the envelope curve for the changes in water storage depicted through orange bars fluctuate accordingly, Fig. 12). For comparison, the automatic separation method from Pelletier and Andréassian (2020) was applied with a quadratic reservoir using their '*baseflow*' R package and adapted to hourly streamflow observations. Using their method, the resulting baseflow responses (dashed light blue line, Fig. 12) appeared much more similar for both watersheds in terms of amplitude and timing than suggested by WRF-Hydro, which calls for further investigation.

Land occupations of these two watersheds are completely different: the upper Dumbea includes forest, dense shrubland and open shrubland. It is devoid of mines. The Coulée watershed includes several abandoned mines and was subjected to repeated wildfires, which both induced severe erosion and gullies reaching the host rock (Fig. 13). Hence, even though it actually includes numerous bare fractured rocks leading to large infiltration of rainwater, the pedology map on which WRF-Hydro's soil types are based inappropriately indicates clay soils for Coulée resulting in low infiltration and percolation capacities. The model thus compensated by adjusting the

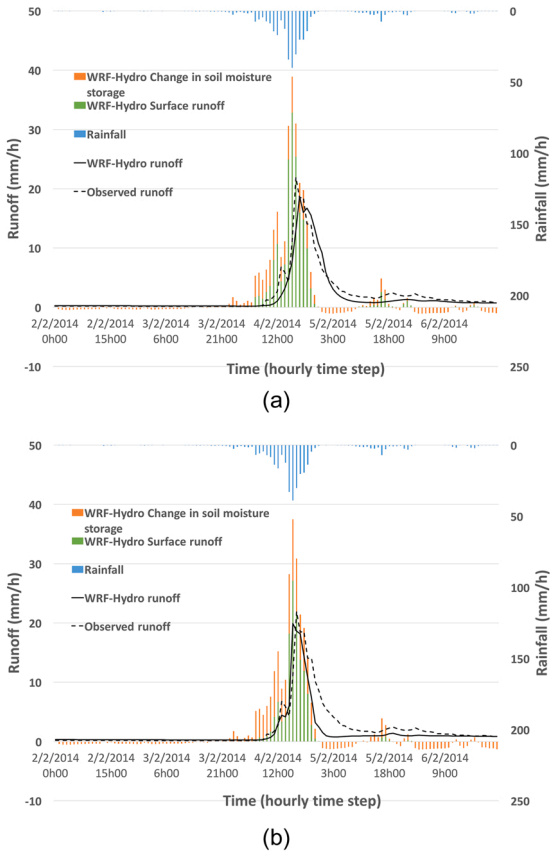


**Fig. 11.** Hourly water budget from rainfall (vertical bars), observed (dashed) and simulated (solid line) hydrograph of the Dumbéa Est watershed depending on the rainfall interpolation method used for calibration and simulation for event 3. Panel (a) uses Thiessen interpolation and (b) uses IDEW method.

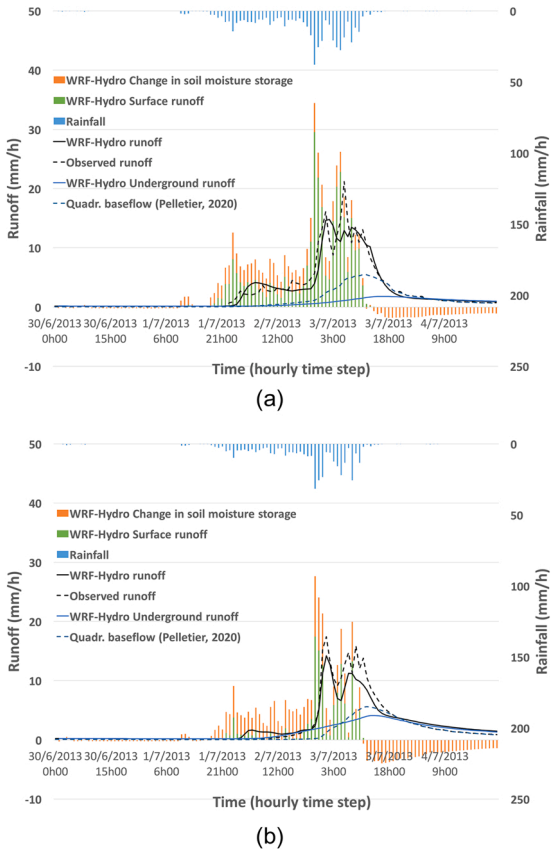


**Fig. 12.** Hourly water budget, observed and simulated hydrograph with baseflow separation as computed by WRF-Hydro (solid light blue line) and with Pelletier and Andréassian (2020)'s method based on observations (dashed light blue line) for event 1. (a) Dumbéa Est – Thiessen method; 472 mm of total rainfall within 5 days; (b) Coulée - Thiessen method; 359 mm of total rainfall within 5 days.

infiltration parameter KDT to 5.0 $day^{-1}$ for Coulée (which is the largest for our six watersheds) and up to 8.9 $day^{-1}$ when tested with IDEW rainfall distribution. In turn, in accordance with its low recession time (43 days, the lowest of all six) and rather high runoff coefficient (61%), percolation from highly infiltrating soil layers to the underground buckets was also boosted almost to its maximum value (SLOPE parameter to 0.98). Eventually, WRF-Hydro was then able to account for the large component of baseflow in Coulée watershed (Fig. 12b). Such a behavior was not suggested for Dumbéa Est by WRF-Hydro (Fig. 12a). The comparison with Pelletier and Andréassian's automatic method which does not show the same baseflow differences between the two watersheds emphasizes some of the strengths of distributed models allowing to better comprehend underground mechanisms in that case.

To further pursue on the advantages stemming from the use of such physics-based model, Fig. 14 shows a similar approach on Thio and Tontouta, the two largest watersheds of our sample. Their hydrographs together with a representation of the time variation of spatial distribution of soil water content allows exploring hydrological spatial behaviors. As mentioned before, Tontouta has a recession time almost twice as important as Thio according to Alric (2009), which resulted in a higher infiltration rate (4–5 times larger than Thio) and lower pore size distribution index and percolation coefficient. Indeed, in Tontouta, the high infiltration coefficient induced a fast absorption of rainwater which long remained stored in elevated areas largely covered with dense forests over clay soils, resulting in slow discharge into the streamflow. Concurrently, water stored within sandy clay loam soils in valleys was rapidly discharged into the stream network bolstering an early baseflow response between $t_0 + 3$ and $t_0 + 5$ days (Fig. 14a and Fig. 7 for groundwater outflow). In contrast, Thio infiltrated less quickly and most of rainwater was thus converted to surface runoff (green bars, Fig. 14b). Its baseflow was consequently slower and much smaller than in Tontouta (see soil moisture maps between $t_0 + 3$ and $t_0 + 5$ days, Fig. 14b).

Comparison with baseflow from Pelletier and Andréassian's automatic separation method (Fig. 12 and Fig. 14) revealed that WRF-Hydro relies much less on underground discharge for flood simulation (except for Coulée). The approach discussed above could however contribute to providing consistent methods for flood decomposition, which still constitutes an open topic (see for example Pelletier and Andréassian, 2020). For instance, a distributed physical model such as WRF-Hydro could help to understand the fate of tracers of harmful minerals in the environment (Arnault et al., 2021).

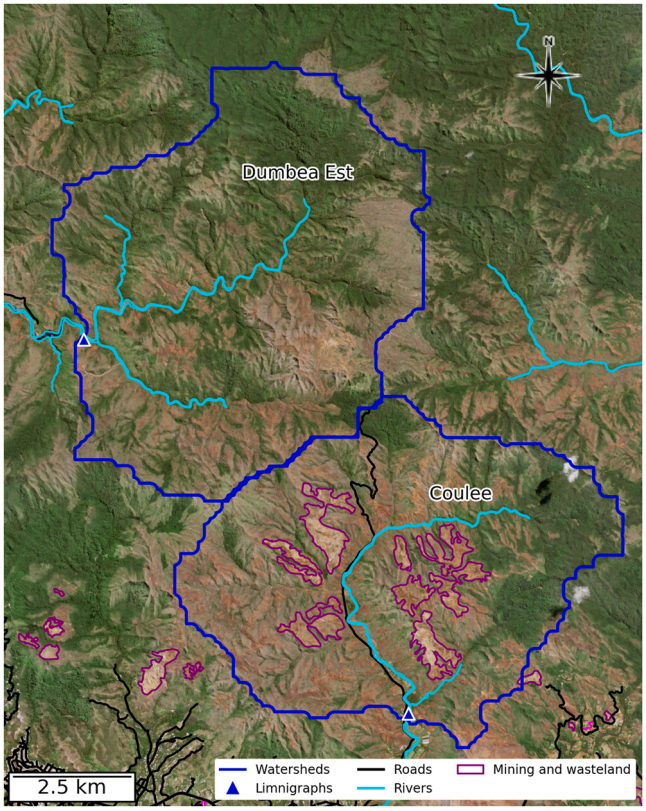


**Fig. 13.** Landsat 8 true color image showing the preserved Dumbéa Est drainage basin and degraded Coulée basin. Old mining sites and others mining wastelands are outlined in purple, using the last Land Cover Model provided by the Government of New Caledonia (MOS 2014, www.georep.nc).

### *5.2. Sensitivity of WRF-Hydro to observed rainfall spatial interpolation method*

Data scarcity for precise rainfall amount and its spatial distribution is generally considered a major source of uncertainties in hydrological modeling (Smith et al., 2004a, 2004b; Moradkhani and Sorooshian, 2009). The two methods of rainfall interpolation resulted in small differences in the NSE on three watersheds, a result already found by Desclaux et al. (2018). Replication of flash-floods (especially recessions) turned out to be slightly poorer with IDEW on the small and highly rainfed Coulée and Dumbéa watersheds with high runoff coefficient ($> 60\%$). Still, since IDEW produced more rainfall on elevated areas, water budgets were changed with generally more water stored in soils during flash-floods. It results that the rainfall interpolation method is likely to control water available for the river when simulating low flow in dry season periods. Accurate rainfall products should thus be used to model the water resource and its evolution under climate change. The larger, flatter and less elevated Pouembout watershed with lower rainfall ($\sim$ 1500 mm/year) and runoff coefficient (27%) displayed a contrasted, more adequate reaction towards peak flow observations with IDEW forcing. Hence, high-resolution rainfall distribution is also crucial for correct flash-flood simulation depending on watershed size and configuration. Generally speaking, for a fixed small number of rain stations, higher sensitivity to spatial distribution and quality of rainfall data is expected with increasing size of watersheds (Hohmann et al., 2021). The validity of the different rainfall interpolation methods could further be explored if refined rainfall data were available thanks to a temporary denser rain gauge network. Finally, the use of DDS calibration with the two interpolation methods also indicated interesting features of WRF-Hydro. When applying IDEW rainfall forcing compared to the Thiessen polygon method, rainfall increase on high areas which are far from the gauging station was relevantly balanced by a decrease in the adjusted Manning and overland flow roughness factors. It indeed allowed surface and channel flow to be accelerated so as to ensure similar and appropriate timing in the triggering of the flood. Overall, large compensation effects were broadly observed between several optimal parameters like KDT compared to BEXP and SLOPE. Calibrated parameter sets are thus the result of model adaptation to multiple sources of errors such as (i) rainfall and streamflow measurements; (ii) weaknesses in the calibration process; (iii) quality of terrestrial data and (iv) flaws in the WRF-Hydro model structure.

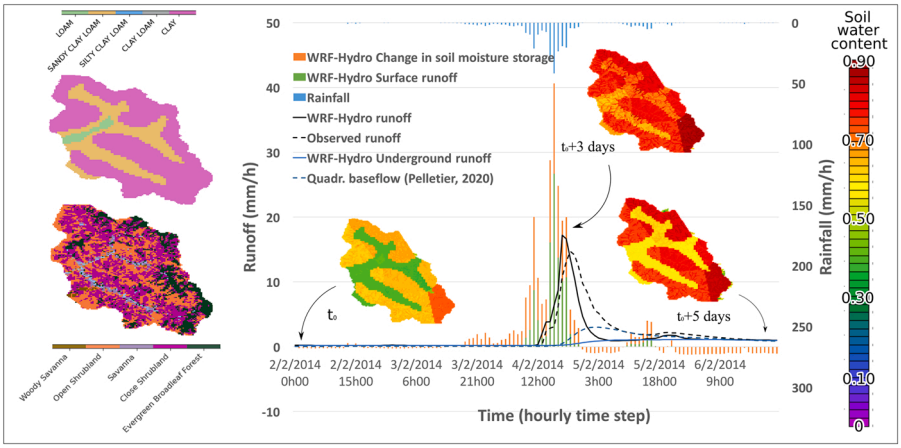


(a)

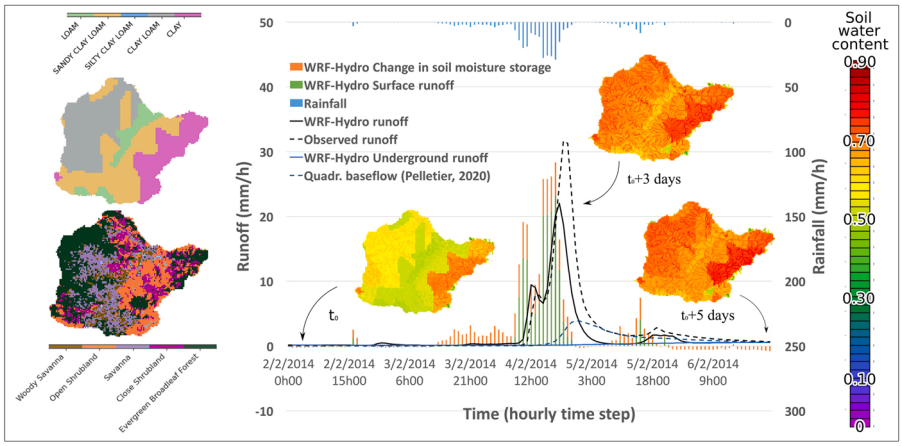


(b)

**Fig. 14.** Hourly water budget, observed and simulated hydrograph with baseflow separation as computed by WRF-Hydro (solid light blue line) and with Pelletier and Andréassian (2020) method based on observations (dashed light blue line). Spatial distribution of soil water content simulated by WRF-Hydro during the Edna tropical depression (event 3). (a) Tontouta - Thiessen method; 277 mm of total rainfall within 5 days; (b) Thio – Thiessen method; 312 mm mm of total rainfall within 5 days.

### *5.3. Significance of optimal physical parameters, benefits, limitations and perspectives of the model in the general context of hydrological modeling*

Following calibration on each of the three short rainfall events and optimal selection of the best 2-year resulting run, WRF-Hydro's final adjusted parameters were found in adequacy with known hydrologic and morphometric properties of watersheds. Indeed, basins with long recession periods were logically attributed low percolation rates (SLOPE) and small pore size distribution (BEXP) in order to simulate slow vertical routing within deep soil layers and thus long-lasting baseflows. High proportion of woody savanna land cover was logically associated with high overland roughness. It was also related to large soil moisture storage which could indicate that maximum water content of soils covered by savanna needed to be adjusted upwards. Manning coefficient was maximum for small mountainous basins characterized by steep rivers with rough beds (Coulée, Dumbéa, Couvelée), while larger watersheds presenting more smooth bed had a lower Manning (Pouembout, Thio, Tontouta). This parameter was highly correlated with rainfall, since high altitude catchments not only receive more rainfall but also correspond to steep slopes and to rough riverbeds. Neither the 2D roughness multiplicative factor, nor the 2D roughness average over the whole watershed (not shown) presented strong correlation with land occupation. A possible explanation could be that surface runoff scarcely occurs and that flow is rather collected in series of gullies. Further evidence of this concentrated flow regime resulted from the fact that all calibrated multiplicative factors were lower than one, implying faster transfer of water than in the default framework. High infiltration coefficients were found for some watersheds with a high clay soil type proportion, indicating a necessary adjustment of the model default behavior, as seen in Section 5.1 for Coulée.

Watersheds presenting a high level of runoff were better described by the model than those presenting both surface runoff and large infiltration. This probably indicates that surface flow is more adequately described by the diffusive wave equation and that the coupling between the surface and subsurface vertical and horizontal routes involves more complex modeling. The latter model

parameterizations suffer from uncertainties in soil parameters and simplification of the supply from soil to the river. Performance analysis on longer time periods should be undertaken to investigate low flow regimes more closely. This would require exploring the sensitivity of the model to the different underground options (only the "pass-through" option was tested here), to the spatial variability of soil thickness and to the agreement of simulated evapotranspiration series, for example to reliable in-situ or satellite data.

Lumped reservoir models such as the GR suite (*modèles du Génie Rural*, Perrin et al., 2009, e.g. GR4H) are able to produce better results on longer time periods in terms of flood simulation (NSE of 0.72 for Coulée, 0.89 for Dumbéa Est and 0.93 for Couvelée in Desclaux et al., 2018) and especially low flow regimes (KGE of the same magnitude). They also require much less human and computational work. However, they need a significant number of years of observations to be properly calibrated. The use of DDS calibration was found efficient for producing good calibrated solutions with few rainfall and streamflow observations (week-long events) while sparing computational work. Owing to this algorithm, WRF-Hydro can be achieved at the scale of small watersheds (few hundred $km^2$) with reasonable spatial resolution (100 m routing grid) and at an hourly time-step onto standard computing systems. In addition, such a physics-based distributed modeling system allows substantially deeper understanding of hydrological processes in the different catchments as well as the ability to easily account for modifications in soil properties and land use, which cannot be achieved in simple reservoir models.

This study started to shed some light on the potential to transfer physical parameters from calibrated watersheds to other ungauged basins in *Grande Terre*. On the one hand, some watersheds with analogous properties shared comparable calibrated values in model parameters. For instance, Couvelée and Tontouta both featured high recession times and moderate runoff coefficients (Table 1). In connection with these characteristics, both were modeled with high infiltration rate KDT combined to low BEXP and SLOPE (Table 3), so as to reproduce large water storage capacity during storms and lasting baseflows during post storm periods. They also both had low OVROUGHRTFAC so as to accelerate surface runoff and balance their large infiltration capacities. Therefore, depending on recession times and runoff coefficients, combinations of low/high KDT opposed to high/low BEXP and SLOPE could be suggested for ungauged basins. On the other hand, it was shown that two closely related watersheds like Coulée and Dumbéa, although sharing some resembling hydrological and environmental features (Table 1), could not be modeled with similar parameters, pointing to difficulties in achieving robust regionalization with WRF-Hydro. Finally, a full spatial distribution of the core parameters selected (KDT, BEXP, SLOPE, OVROUGHRTFAC, MANN and $SMC_{MAX}$) could allow for a better transition at watershed boundaries and improve regionalization perspectives.

Although suitable simulation was performed and insightful developments were allowed, limitations of this work remain present. First of all, even though the chosen period of calibration/validation encompasses many of the climate features of the region, results necessarily bear dependencies to the data, even more so as the simulation and validation periods are rather short (3 weeks and 2 years). Parameter values may presumptively be contingent to the selection and length of calibration events. Moreover, the validation period only partly accounts for the decennial climatic variability of New Caledonia. In addition to using short flash-flood calibration periods, the multi-objective function used here gives more weight to high flows and thus influences the ultimate setup of the model. Low flows appear to be reproduced in a much less satisfactory way than high flows in our framework, especially on Couvelée and Pouembout. Two exogenous additive factors that are not controlled by the calibration process could explain an upward bias in simulated low flows, especially when working at an hourly time step: (i) evapotranspiration is likely underestimated in wet tropical environments by WRF-Hydro (Lin et al., 2018) and (ii) rain gauge spatial interpolation may introduce too much water in the system, including in low rainfall periods (Schleiss et al., 2020). All in all, even though WRF-Hydro was found to be suitable to simulate flash-flood patterns in various basins of New Caledonia, this study's interpretations remain conditional to the testing conditions and thus have to be taken with caution.

## 6. Summary and conclusion

In this study, the WRF-Hydro modeling framework was found able to fairly simulate runoff observations and faithfully reproduce flash flood behavior on six watersheds of the tropical island of New Caledonia (SW Pacific). This work focused on a two-year period and made use of a WRF meteorological forcing complemented with spatially interpolated rain gauge data. It achieved good results in terms of NSE after automatic calibration on three short (less than one week) and contrasted events thanks to a workflow based on the DDS algorithm. With alternating moderate El Niño and La Niña periods affected by flash floods during both dry and wet seasons, we believe the calibration/validation time interval chosen in this study was relevant in terms of climatological representativeness of New Caledonia.

Following the analysis of adjusted parameters and simulated water budget components on two flash-flood events, the model successfully reproduced hydrological behavior of all watersheds. It provided fairly matching physical constants with known hydrologic and morphometric properties confirmed by correlation statistics. Yet as these were obtained only on a six-watershed sample, extension of the analysis to other watersheds in New Caledonia should be prioritized in future studies. Longer calibration and simulation periods should also be selected to confirm the conclusions. In some instances, such as the Coulée watershed, WRF-Hydro's adjusted parameters provided perspectives for a better understanding of the watershed properties that were inadequately described in the available soil database. Overall, WRF-Hydro enabled to model some of the diversity of soils and land occupation of *Grande Terre* of New Caledonia. This study thus confirms that WRF-Hydro is relevant for flash-flood analysis on small watersheds even with limited rainfall observations. WRF-Hydro also provided information on distributed properties such as the water budgets and soil humidity. We showed that thanks to a better constraint on the watershed water storage properties, the model allowed discussing most components of the flood signal, including its recession part. Thanks to its decomposition of runoff components, WRF-Hydro constitutes a fine tool to help better compare subsurface and underground water components between allegedly similar catchments.

It is important to point out that realistic rainfall spatial distribution is needed in order to provide distributed water resources. This was emphasized here by the difference in water budget components between the Thiessen polygon and IDEW rainfall interpolation methods. With the continuous improvements of meteorological models such as WRF allowing small scale representation of atmospheric variables, there are hopes that flood events and their dynamics can be better understood. Along the same lines, the framework that we have developed may be used to understand how climate variability and climate change can impact water resources in New Caledonia, especially in the context of a drastic projected drying of New Caledonia by the end of the century. We finally suggest that the findings of the present study could also be conclusive on other mountainous islands presenting watersheds similar in size and in altitude to those of *Grande Terre* and experiencing comparable weather conditions.

## Declaration of Competing Interest

The authors declare that they have no known competing financial interests or personal relationships that could have appeared to influence the work reported in this paper.

## Acknowledgements

The authors would like to thank T. Delahaye (IRD) for technical development, C. Laroche and most of all M. Chauveau from *Direction des Affaires Vétérinaires, Alimentaires et Rurales* (DAVAR) for precious research guidance. We also thank Romain Legendre (IFREMER) who helped us in providing data and other unpublished results based on GR4H. This work was supported by CNRS Grant from CNRS-MITI for CYCLOP project.

## References

Alric, R., 2009. Recueil des débits caractéristiques de la Nouvelle-Calédonie. DAVAR, Nouméa.
Arnaud, P., Bouvier, C., Cisneros, L., Dominguez, R., 2002. Influence of rainfall spatial variability on flood prediction. J. Hydrol. 260 (1–4), 216–230. https://doi.org/10.1016/S0022-1694(01)00611-4.
Arnault, J., Rummler, T., Baur, F., Lerch, S., Wagner, S., Fersch, B., Zhang, Z., Kerandi, N., Keil, C., Kunstmann, H., 2018. Precipitation sensitivity to the uncertainty of terrestrial water flow in WRF-Hydro: an ensemble analysis for central Europe. J. Hydrometeorol. 19, 1007–1025.
Arnault, J., Jung, G., Haese, B., Fersch, B., Rummler, T., Wei, J., Zhang, Z., Kunstmann, H., 2021. A joint soil-vegetation-atmospheric modeling procedure of water isotopologues: implementation and application to different climate zones with WRF-Hydro-iso. J. Adv. Model. Earth Syst. 13 (10) https://doi.org/10.1029/2021MS002562 (e2021MS002562).
Arsenault, R., Poulin, A., Côté, P., Brissette, F., 2014. Comparison of stochastic optimization algorithms in hydrological model calibration. J. Hydrol. Eng. 19 (7), 1374–1384. https://doi.org/10.1061/(ASCE)HE.1943-5584.0000938.
Barbero, R., Moron, V., Mangeas, M., Despinoy, M., Hély, C., 2011. Relationships between MODIS and ATSR fires and atmospheric variability in New Caledonia (SW Pacific). J. Geophys. Res. 116 (D21110) https://doi.org/10.1029/2011JD015915.
Beck, H.E., van Dijk, A.I.J.M., de Roo, A., Miralles, D.G., Mc Vicar, T.R., Schellekens, J., Bruijnzee, L.A., 2016. Global-scale regionalization of hydrologic model parameters. Water Resour. Res. 52 (5), 3599–3622. https://doi.org/10.1002/2015WR018247.
Bénichou, P., Le Breton, O., 1987. AURELHY: une méthode d'analyse utilisant le relief pour les besoins de l'hydrométéorologie. In: Deuxièmes journées hydrologiques de l'ORSTOM à Montpellier. ORSTOM, Paris, pp. 299–304 ((Colloques et Séminaires). ISBN 2-7099-0865-4. ISSN 0767-2896).
Beven, K.J., 2000. Rainfall runoff modelling. The primer. Wiley, Chichester, UK, p. 372.
Bierque, E., Thibeaux, R., Girault, D., Soupé-Gilbert, M.-E., Goarant, C., 2020. A systematic review of Leptospira in water and soil environments. PLoS One 15, e0227055. https://doi.org/10.1371/journal.pone.0227055.
Camera, C., Bruggeman, A., Zittis, G., Sofokleous, I., Arnault, J., 2020. Simulation of extreme rainfall and streamflow events in small Mediterranean watersheds with a one-way-coupled atmospheric–hydrologic modelling system. Nat. Hazards Earth Syst. Sci. 20 (10), 2791–2810. https://doi.org/10.5194/nhess-20-2791-2020.
Ceccarelli, D.M., McKinnon, A.D., Andréfouët, S., Allain, V., Young, J., Gledhill, D., C, Flynn, A., Bax, N.J., Beaman, R., Borsa, P., Brinkman, R., Bustamante, R.H., Campbell, R., Cappo, M., Cravatte, S., D'Agata, S., Dichmont, C.M., Dunstan, P.K., Dupouy, C., Edgar, G., Farman, R., Furnas, M., Garrigue, C., Hutton, T., Kulbicki, M., Letourneur, Y., Lindsay, D., Menkes, C., Mouillot, D., Parravicini, V., Payri, C., Pelletier, B., Richer de Forges, B., Ridgway, K., Rodier, M., Samadi, S., Schoeman, D., Skewes, T., Swearer, S., Vigliola, L., Wantiez, L., Williams, Alan, Williams, Ashley, Richardson, A.J., 2013. Chapter four – the coral sea: physical environment, ecosystem status and biodiversity assets. Adv. Mar. Biol. 66, 213–290. https://doi.org/10.1016/B978-0-12-408096-6.00004-3.
Charlier, J.B., Cattan, P., Moussa, R., Voltz, M., 2008. Hydrological behaviour and modelling of a volcanic tropical cultivated catchment. Hydrol. Process. 22 (22), 4355–4370. https://doi.org/10.1002/hyp.7040.
Chen, F., Mitchell, K.E., Schaake, J., Xue, Y., Pan, H.-L., Koren, V., Duan, Q.Y., Ek, M., Betts, A., 1996. Modeling of land-surface evaporation by four schemes and comparison with FIFE observations. J. Geophys. Res. 101 (D3), 7251–7268. https://doi.org/10.1029/95JD02165.
Cuo, L., Pagano, T.C., Wang, Q.J., 2011. A review of quantitative precipitation forecasts and their use in short- to medium-range streamflow forecasting. J. Hydrometeorol. 12 (5), 713–728. https://doi.org/10.1175/2011JHM1347.1.
David, G., Leopold, M., Dumas, P.S., Ferraris, J., Herrenschmidt, J.B., Fontenelle, G., 2010. Integrated coastal zone management perspectives to ensure the sustainability of coral reefs in New Caledonia. Mar. Pollut. Bull. 61 (7–12), 323–334. https://doi.org/10.1016/j.marpolbul.2010.06.020.
Desclaux, T., Lemonnier, H., Genthon, P., Soulard, B., Le Gendre, R., 2018. Suitability of a lumped rainfall-runoff model for flashy tropical watersheds in New Caledonia. Hydrol. Sci. J. 63 (11), 1689–1706. https://doi.org/10.1080/02626667.2018.1523613.
Dupouy, C., Wattelez, G., Lefèvre, J., Juillot, F., Andréoli, R., Lille, D., Murakami, H., Röttgers, R., Frouin, R., 2018. Rain-derived particles and CDOM distribution along the east coast of New Caledonia. Remote Sensing of the Open and Coastal Ocean and Inland Waters, Proc. SPIE 10778. ⟨https://doi.org/10.1117/12.2501807⟩.
Dutheil, C., Bador, M., Lengaigne, M., Lefèvre, J., Jourdain, N.C., Vialard, J., Jullien, S., Peltier, A., Menkes, C., 2019. Impact of surface temperature biases on climate change projections of the South Pacific Convergence Zone. Clim. Dyn. 53, 3197–3219. https://doi.org/10.1007/s00382-019-04692-6.
Dutheil, C., Lengaigne, M., Bador, M., Vialard, J., Lefèvre, J., Jourdain, N.C., Jullien, S., Peltier, A., Sultan, B., Menkès, C., 2020a. Impact of projected sea surface temperature biases on tropical cyclones projections in the South Pacific. Sci. Rep. 10, 4838. https://doi.org/10.1038/s41598-020-61570-6.
Dutheil, C., Menkes, C., Lengaigne, M., Vialard, J., Peltier, A., Bador, M., Petit, X., 2020b. Fine-scale rainfall over New Caledonia under climate change. Clim. Dyn. 56, 87–108. https://doi.org/10.1007/s00382-020-05467-0.
Fares, A. 2008. Overview of the hydrological modeling of small coastal watersheds on tropical islands. Coastal Watershed Management. International Series on Progress in Water Resources. WIT Press, vol. 33. ⟨https://doi.org/10.2495/978-1-84564-091-0/01⟩.
Fares, A., Awal, R., Michaud, J., Chu, P.-C., Fares, S., Kodoma, K., Rosener, M., 2014. Rainfall-runoff modeling in a flashy tropical watershed using the distributed HL-RDHM model. J. Hydrol. 519 (D), 3436–3447. https://doi.org/10.1016/j.jhydrol.2014.09.042.

Fisher, R.A., Yates, F., 1953. Statistical Tables for Biological, Agricultural and Medical Research. Oliver and Boyd, London, p. 126.
Fritsch, E., 2012. Les sols. Atlas de la Nouvelle Calédonie. Marseille; Nouméa: IRD; Congrès de la Nouvelle-Calédonie, 73–76. ISBN 978-2-7099-1740-1. ⟨http://horizon.documentation.ird.fr/exl-doc/pleins_textes/divers20-04/010058388.pdf⟩.
Frysou, O., 2008. Caractérisation des régimes d'étiage en Nouvelle Calédonie, DAVAR, Nouméa. 183 pp. ⟨https://davar.gouv.nc/sites/default/files/atoms/files/caracterisation_des_regimes_detiage_en_nouvelle-caledonie.pdf⟩.
Gochis, D.J., Chen, F., 2003. Hydrological enhancements to the community Noah Land Surface Model. NCAR Technical Document. ⟨https://doi.org/10.5065/D60P0X00⟩.
Gochis, D.J., Yu, W., Yates, D.N., 2013. The WRF-Hydro Model Technical Description and User's Guide, Version 1.0. NCAR Technical Document. 120 pp. ⟨https://ral.ucar.edu/sites/default/files/public/projects/wrf_hydro/WRF_Hydro_Technical_Description_and%20User_Guide_v1.0.pdf⟩.
Gupta, H., Kling, H., Yilmaz, K., Martinez, G., 2009. Decomposition of the mean squared error and NSE performance criteria: implications for improving hydrological modelling. J. Hydrol. 377, 80–91. https://doi.org/10.1016/j.jhydrol.2009.08.003.
Hingray, B., Picouet, C., Musy, A., 2015. Hydrology: A Science for Engineers. CRC Press, Boca Raton, USA, p. 612.
Hohmann, C., Kirchengast, G., Sungmin, O., Rieger, W., Foelsche, U., 2021. Small catchment runoff sensitivity to station density and spatial interpolation: hydrological modeling of heavy rainfall using a dense rain gauge network. Water 13 (10), 1381. https://doi.org/10.3390/w13101381.
Jourdain, N.C., Marchesiello, P., Menkes, C.E., Lefèvre, J., Vincent, E.M., Lengaigne, M., Chauvin, F., 2011. Mesoscale simulation of tropical cyclones in the south pacific: climatology and interannual variability. J. Clim. 24 (1), 3–25. https://doi.org/10.1175/2010JCLI3559.1.
Jullien, S., Marchesiello, P., Menkes, C., Lefèvre, J., Jourdain, N.C., Samson, G., Lengaigne, M., 2014. Ocean feedback to tropical cyclones: climatology and processes. Clim. Dyn. 43, 2831–2854. https://doi.org/10.1007/s00382-014-2096-6.
Karsten, L., 2018. Overview of Model Calibration General Strategy & Optimization. NCAR Technical document. ⟨https://ral.ucar.edu/sites/default/files/public/9CalibrationOverview_2018Karsten.pdf⟩.
Kobold, M., Suselj, K., 2005. Precipitation forecasts and their uncertainty as input into hydrological models. Hydrol. Earth Syst. Sci. 9 (4), 322–332. https://doi.org/10.5194/hess-9-322-2005.
Lafarge, W., Lefèvre, J., Despinoy, M., Isnard, S., Menkes, C., 2014. Classification exploitable pour le projet CLiveNC, traitements de données MODIS et carte des sols en Nouvelle-Calédonie. Rapp. Intern. IRD/Ocean. 20.
Lefèvre, J., Marchesiello, P., Jourdain, N., Menkès, C., Leroy, A., 2010. Weather regimes and orographic circulation around New Caledonia. Mar. Pollut. Bull. 61 (7–12), 413–431. https://doi.org/10.1016/j.marpolbul.2010.06.012.
Lin, P., Rajib, M.A., Yang, Z.-L., Somos-Valenzuela, M., Merwade, V., Maidment, D.R., Wang, Y., Chen, L., 2018. Spatiotemporal evaluation of simulated evapotranspiration and streamflow over Texas using the WRF-Hydro-RAPID modeling framework. J. Am. Water Resour. Assoc. 54 (1), 40–54. https://doi.org/10.1111/1752-1688.12585.
Masih, I., Maskey, S., Uhlenbrook, S., Smakhtin, V., 2011. Assessing the impact of areal precipitation input on streamflow simulations using the SWAT Model. J. Am. Water Resour. Assoc. 47 (1), 179–195. https://doi.org/10.1111/j.1752-1688.2010.00502.x.
Maurizot, P., Vendé-Leclerc, M., 2012. La géologie – Planche 13. In: Bonvallot, J., Gay, J., Habert, E. (Eds.), Atlas de la Nouvelle-Calédonie. IRD, Congrès de la Nouvelle-Calédonie, Marseille-Nouméa.
Moradkhani, H., Sorooshian, S., 2009. General review of rainfall-runoff modeling: model calibration, data assimilation, and uncertainty analysis. In: Sorooshian, S., Hsu, K.L., Coppola, E., Tomassetti, B., Verdecchia, M., Visconti, G. (Eds.), Hydrological Modelling and the Water Cycle. Water Science and Technology Library, 63. Springer, Berlin, Heidelberg. https://doi.org/10.1007/978-3-540-77843-1_1.
Moriasi, D.N., Arnold, J.G., Van Liew, M.W., Bingner, R.L., Harmel, R.D., Veith, T.L., 2007. Model evaluation guidelines for systematic quantification of accuracy in watershed simulations. Trans. ASABE 50 (3), 885–900. https://doi.org/10.13031/2013.23153.
Moron, V., Barbero, R., Robertson, A.W., 2016. Subseasonal-to-interannual variability of rainfall over New Caledonia (SW Pacific). Clim. Dyn. 46, 2449–2468. https://doi.org/10.1007/s00382-015-2712-0.
Niu, G.-Y., Yang, Z.-L., Mitchell, K.E., Chen, F., Ek, M.B., Barlage, M., Kumar, A., Manning, K., Niyogi, D., Rosero, E., Tewari, M., Xia, Y., 2011. The community Noah land surface model with multiparameterization options (Noah-MP): 1. Model description and evaluation with local-scale measurements. J. Geophys. Res. 116 (D12) https://doi.org/10.1029/2010JD015139.
Payri, C.E., Allain, V., Aucan, J., David, C., David, V., Dutheil, C., Loubersac, L., Menkes, C., Pelletier, B., Pestana, G., Samadi, S., 2019. Chapter 27 – New Caledonia. In: Sheppard, C. (Ed.), World Seas: An Environmental Evaluation, Second edition. Academic Press, pp. 593–618. https://doi.org/10.1016/B978-0-08-100853-9.00035-X.
Pelletier, A., Andréassian, V., 2020. Hydrograph separation: an impartial parametrisation for an imperfect method. Hydrol. Earth Syst. Sci. 24 (3), 1171–1187. https://doi.org/10.5194/hess-24-1171-2020.
Perrin, C., Michel, C., Andréassian, V., 2009. A set of hydrological models (chapter 16). In: Tanguy, J.M. (Ed.), Environmental Hydraulics, 279. ISTE Ltd, John Wiley and Sons, Paris, pp. 493–509, 2009.
Richmond, R.H., Rongo, T., Golbuu, Y., Victor, S., Idechong, N., Davis, G., Kostka, W., Neth, L., Hamnett, M., Wolanski, E., 2007. Watersheds and coral reefs: conservation science, policy, and implementation. BioScience 57 (7), 598–607. https://doi.org/10.1641/B570710.
Rummler, T., Arnault, J., Gochis, D.J., Kunstmann, H., 2019. Role of lateral terrestrial water flow on the regional water cycle in a complex terrain region: Investigation with a fully coupled model system. J. Geophys. Res. Atmos. 124 (2), 507–529. https://doi.org/10.1029/2018JD029004.
Schleiss, M., Olsson, J., Berg, P., Niemi, T., Kokkonen, T., Thorndahl, S., Nielsen, R., Nielsen, J.E., Bozhinova, D., Pulkkinen, S., 2020. The accuracy of weather radar in heavy rain: a comparative study for Denmark, the Netherlands, Finland and Sweden. Hydrol. Earth Syst. Sci. 24, 3157–3188. https://doi.org/10.5194/hess-24-3157-2020.
Senatore, A., Mendicino, G., Gochis, D.J., Yu, W., Yates, D.N., Kunstmann, H., 2015. Fully coupled atmosphere-hydrology simulations for the central Mediterranean: impact of enhanced hydrological parameterization for short and long time scales. J. Adv. Model. Earth Syst. 7 (4), 1693–1715. https://doi.org/10.1002/2015MS000510.
Skamarock, W.C., Klemp, J.B., Dudhia, J., Gill, D.O., Barker, D., Duda, M.G., Huang, X.-Y., Wang, W., Powers, J.G., 2008. A Description of the Advanced Research WRF Version 3 (No. NCAR/TN-475 + STR). NCAR Technical Report. University Corporation for Atmospheric Research. ⟨https://doi.org/10.5065/D68S4MVH⟩.
Smith, M.B., Seo, D.-J., Koren, V.I., Reed, S.M., Zhang, Z., Duan, Q., Moreda, F., Cong, S., 2004a. The distributed model intercomparison project (DMIP): motivation and experiment design. J. Hydrol. 298 (1–4), 4–26. https://doi.org/10.1016/j.jhydrol.2004.03.040.
Smith, M.B., Koren, V.I., Zhang, Z., Reed, S.M., Pan, J.-J., Moreda, F., 2004b. Runoff response to spatial variability in precipitation: an analysis of observed data. J. Hydrol. 298 (1–4), 267–286. https://doi.org/10.1016/j.jhydrol.2004.03.039.
Smith, M.B., Koren, V.I., Reed, S.M., Zhang, Z., Moreda, F., Cui, Z., Mizukami, N., Anderson, E.C., Cosgrove, A.C., 2012. The distributed model intercomparison project – phase 2: motivation and design of the Oklahoma experiments. J. Hydrol. 418–419, 3–16. https://doi.org/10.1016/j.jhydrol.2011.08.055.
Strauch, A.M., MacKenzie, R.A., Giardina, C.P., Bruland, G.L., 2015. Climate driven changes to rainfall and streamflow patterns in a model tropical island hydrological system. J. Hydrol. 523, 160–169. https://doi.org/10.1016/j.jhydrol.2015.01.045.
Terry, J.P., Wotling, G., 2011. Rain-shadow hydrology: influences on river flows and flood magnitudes across the central massif divide of La Grande Terre Island, New Caledonia. J. Hydrol. 404 (1–2), 77–86. https://doi.org/10.1016/j.jhydrol.2011.04.022.
Tolson, B.A., Shoemaker, C.A., 2007. Dynamically dimensioned search algorithm for computationally efficient watershed model calibration. Water Resour. Res. 43, W01413 https://doi.org/10.1029/2005WR004723.
Tramier, C., Genthon, P., Delvienne, Q., Sauvan, N., Cassan, J.-J., Ebrard, E., Dumas, P., Queffélean, Y., 2021. Hydrological regimes in a tropical valley of New Caledonia (SW Pacific): impacts of wildfires and invasive fauna. Hydrol. Process. 35 (3), e14071 https://doi.org/10.1002/hyp.14071.
Verri, G., Pinardi, N., Gochis, D.J., Tribbia, J., Navarra, A., Coppini, G., Vukicevic, T., 2017. A meteohydrological modelling system for the reconstruction of river runoff: the case of the Ofanto river catchment. Nat. Hazards Earth Syst. Sci. 17, 1741–1761. https://doi.org/10.5194/nhess-17-1741-2017.

Wotling, G., 2000. Caractérisation et modélisation de l'aléa hydrologique à Tahiti (Ph.D. Thesis). Univ. Montpellier France. ⟨https://horizon.documentation.ird.fr/exl-doc/pleins_textes/divers16-09/010020486.pdf⟩.

Xu, X., Frey, S.K., Boluwade, A., Erler, A.R., Khader, O., Lapen, D.R., Sudicky, E., 2019. Evaluation of variability among different precipitation products in the Northern Great Plains. J. Hydrol.: Reg. Stud. 24, 100608 https://doi.org/10.1016/j.ejrh.2019.100608.

Yochum, S., Bledsoe, B., David, G., Wohl, E., 2012. Velocity prediction in high-gradient channels. J. Hydrol. 424–425, 84–98. https://doi.org/10.1016/j.jhydrol.2011.12.03.

Yucel, I., Onen, A., Yilmaz, K.K., Gochis, D.J., 2015. Calibration and evaluation of a flood forecasting system: utility of numerical weather prediction model, data assimilation and satellite-based rainfall. J. Hydrol. 523, 49–66. https://doi.org/10.1016/j.jhydrol.2015.01.042.